

December 2020

Scaling and Entropic Approaches to Clusters in Materials Science and in Network

Prosun Roy
University of Wisconsin-Milwaukee

Follow this and additional works at: <https://dc.uwm.edu/etd>



Part of the [Mechanical Engineering Commons](#)

Recommended Citation

Roy, Prosun, "Scaling and Entropic Approaches to Clusters in Materials Science and in Network" (2020).
Theses and Dissertations. 2589.
<https://dc.uwm.edu/etd/2589>

This Thesis is brought to you for free and open access by UWM Digital Commons. It has been accepted for inclusion in Theses and Dissertations by an authorized administrator of UWM Digital Commons. For more information, please contact open-access@uwm.edu.

**SCALING AND ENTROPIC APPROACHES TO
CLUSTERS IN MATERIALS SCIENCE AND IN
NETWORKS**

by

Prosun Roy

**A Thesis Submitted in
Partial Fulfillment of the
Requirements for the Degree of**

**Master of Science
in Engineering**

at

The University of Wisconsin-Milwaukee

December 2020

ABSTRACT

SCALING AND ENTROPIC APPROACHES TO CLUSTERS IN MATERIALS SCIENCE AND IN NETWORKS

by

Prosun Roy

**The University of Wisconsin-Milwaukee, 2020
Under the Supervision of Dr. Michael Nosonovsky**

The thesis we have studied, is about scaling and entropic content in various networks related to the material science, colloids and biological systems. The thesis is based on two papers:

- Nosonovsky M.; Roy P. Allometric scaling law and ergodicity breaking in the vascular system. *Microfluidics and Nanofluidic-Springer*. **2020** [Chapter 2 and 3]
- Nosonovsky M.; Roy P. Scaling and Entropy in colloidal and neural networks. *Entropy-MPDI*. **2020** [Chapter 5 to 7]

In chapter 2, we investigate scaling properties of vascular networks with fractal topology. Computational fluid dynamic (CFD) simulation of blood flow through one bifurcating vessel has been illustrated to demonstrate that complex dependencies cannot be approximated by a simple allometric scaling law.

In chapter 3, this thesis investigates the ergodicity in the fractal vascular system by suggesting a generalized formulation of branching model. Ergodicity breaking is attributed to the fractal structure of the network as fluid flow in a fractal network system is not ergodic. The fractal branching is viewed as a source of ergodicity breaking in the biomechanical system. It is accounted that ergodicity is significant for a wide range of biomedical application where long observations time series are not practical.

In chapter 4, dimensional and scaling analysis is implemented on networks, which contain fractal, scale-free and small-world properties. The quantity of information contained in a network could be estimated by the calculation of its Shannon entropy. Networks arising from tiny colloidal particles and droplet clusters due to pairwise interaction between the particles, have been considered in our work. In the colloidal science, due to influence of percolation and self-organized critically, networks have self-organizing properties and these properties tune the colloidal particles to the critical state, where system becomes unstable.

In chapter 5, discussion of much more complex networks such neurons, which are organized in neocortex, has been demonstrated. Scaling relationship found in the neocortex suggests that characteristic time constant is independent of brain size when interspecies comparison is analyzed.

In chapter 6, two physical concepts such as self-organizing criticality (SOC) and percolation, relevant to the self-organization of neural networks have been manifested. Then, sand-pile conceptual model of SOC and hypotheses of brain network formation by SOC, have been analyzed. To this end, the role of percolation to trigger avalanche in a system has been stated.

In chapter 7, a review of experimental data about the scaling properties of cortical networks related to their temporal and spatial orientation, has been explored. Then, we extract the

informational content of those cortical networks from entropic viewpoint. Scaling relationship of cortical networks suggest that characteristic time constant (rate of neural process) is independent of the brain size, when interspecies comparison is conducted.

**© Copyright by Prosun Roy, 2020
All Rights Reserved**

TABLE OF CONTENTS

1. Introduction.....	1
2. Allometric law and ergodicity in vascular networks.....	4
2.1. Formulation of the problem.....	4
2.2. Scaling relationships for a branching capillary system.....	6
2.2.1. Branching with area and volume conservation.....	6
2.2.2. Considering more realistic scaling dependencies.....	7
3. Ergodicity breaking analysis.....	10
4. Clusters and networks.....	15
4.1. Networks in Material Science.....	15
4.2. Droplets and colloidal clusters as networks.....	19
5. Multiscale organization of neo-cortex network.....	23
5.1. Organization of neo-cortex: macro-columns and mini-columns.....	23
5.2. Small-world and scale-invariant behavior.....	25
6. Percolation and criticality studies.....	28
6.1. Percolation in materials and in networks.....	28
6.2. Percolation in multiphase systems.....	33
6.3. Percolation and information processing.....	35
7. Scaling in brain networks.....	37
7.1. Some experimental observations on scaling in brain networks.....	37
7.2. Brain rhythms and scaling.....	40
7.3. Information content of the networks.....	44
8.. Conclusions.....	46
9. References.....	48

LIST OF FIGURES

<i>Figure 2.1. Branching of a vascular network; three levels are shown.....</i>	<i>6</i>
<i>Figure 2.2. CFD simulation of blood flow through a bifurcating (branching) vessel shows complex dependencies of velocity, which cannot be approximated by a simple scaling relationship. Velocity contours in (a) perpendicular and (b) parallel cross-section and (c) flow streamlines for the peak systolic phase are shown.....</i>	<i>8</i>
<i>Figure 2.3. Schematic of blood flow in a blood vessel showing layers of the blood vessel and various components of blood. The interaction with the blood vessel wall is important due to its medical significance and hemodynamic effects.....</i>	<i>9</i>
<i>Figure 3.1. (a) Time fraction and (b) ergodicity defect as a function of the volume fraction for three combinations of parameters a and b.....</i>	<i>12</i>
<i>Figure 3.2. Oscillations of a small levitating droplet cluster, which vibrates as a whole.....</i>	<i>14</i>
<i>Figure 4.1. Small world network concept. While some nodes have connections only with their neighbors, edges connecting with remote nodes provide short geodesic paths.....</i>	<i>17</i>
<i>Figure 4.2. Model of jamming in a granular media as percolation of a force network. The force is transmitted through chains of connecting grains shown in black.....</i>	<i>17</i>
<i>Figure 4.3. Apollonian packing and a corresponding graph.....</i>	<i>18</i>
<i>Figure 4.4. A hexagonally ordered 2D droplet cluster levitating over a water surface. The size of the frame is 0.75 mm.....</i>	<i>19</i>
<i>Figure 4.5. Schematic of colloidal particles forming small clusters.....</i>	<i>20</i>
<i>Figure 4.6. Experimental probability distributions of 8-bonds (right part) and 7-bonds (left part) structures. Each point is representing each distinguished structure of colloidal cluster.....</i>	<i>21</i>

Figure 5.1. Neurons and their parts forming a network. (a) The arrangement of neurons, dendrites and axons in vertical modules of the striate cortex of the macaque monkey. (b) The arrangement of the apical dendrites of pyramidal cells in the cortex showing the six layers (I to VI). The cells in layers II to V (red), VI (green), and (IV) (blue, no dendrites) are shown. (c) Columns built of dendrites and axons.....24

Figure 6.1. The sand-pile conceptual model of SOC. The pile tends to have slope angle defined by the friction between grains. Adding one new grain to the pile may have no effect (grain is at rest) or it may cause an avalanche. The magnitude and frequency of avalanches are inversely related.....28

Figure 6.2. Hypotheses of brain network formation by SOC (Kozma et al., 2005). (a) The neocortex network evolves after the birth toward regions of criticality. Once the critical regions (black) are established, the connectivity structure remains essentially unchanged, but it can adjust close to critical regions. (b) Schematic (log-log scale) showing distribution of pyramidal axon tree size. The power law is a typical SOC footprint.....30

Figure 6.3. Percolation. (a) A 2D torus model with a two active neighbors local update rule showing first four iteration steps at the eighth step all sites become active (Bollobas, 2001). (b) A typical dependency of the correlation length on the shear load for an avalanche. At the critical value of the load, σ_0 , the correlation length approaches the infinity. (c) With increasing normal load, the size of slip zone spots (black) increases. A transition to the global sliding is expected when the correlation length approaches the infinity.....31

Figure 6.4. (a) Avalanche size (log-log scale) distributions in brain shows a power-law dependency (b)The activity may decrease, stay at the same level, or grow with time depending on the branching regime.....32

Figure 7.1. The effect of (a) body mass (gram) and (b) temperature-corrected mass-specific resting metabolic rate (qWg) on the CFF shows that the CFF increases with the metabolic rate but decreases with body mass.....39

Figure 7.2. Interspecies scaling relations in brain (based on Wang et al., 2008). (a) Cross-brain conduction times for myelinated axons; (b) the fraction of myelinated axons; (c) the fraction of volume filled by axons; (d) distribution of axon densities.....41

Figure 7.3. Scaling relationship between interspecies brain diameter (cm) and ratio of white & grey matter.....43

LIST OF TABLES

<i>Table 4.1. Structures of 7-bonds colloidal clusters and their magnitudes of probability distribution and Zipf-Law distribution.....</i>	<i>22</i>
<i>Table 4.2. Structures of 8-bonds colloidal clusters and their magnitudes of probability distribution and Zipf-Law distribution.....</i>	<i>22</i>
<i>Table 7.1. Number of neurons, synapses, and corresponding information content of some organisms.....</i>	<i>45</i>

ACKNOWLEDGEMENTS

I would like to express my deep gratitude to my graduate supervisor, *Dr. Michael Nosonovsky*, for his invaluable support and help during my thesis. I would also like to thank *Dr. Mohammad H. Rahman* and *Dr. Junjie Niu* for serving on my graduate committee.

1. Introduction

In recent time, due to the success of computer networks such as the internet, theory of networks, which originates in the mathematical theory of graphs, became a particularly successful and popular method of modelling various processes and systems. Network science can be applied in such diverse areas as the materials science, where they could represent, for example, a force network and packing of granular material, or as the colloidal science where they represent colloidal and droplet crystals. Network description also emerges naturally in the study of biological systems such as the vascular or neural systems, including the brain. Networks as mathematical objects possess certain topological and, in particular, scaling properties. Fractal properties are often related to self-organizing phenomena such as self-organized criticality – a particular type of self-organization, which plays a role in several areas of science from surface science and avalanches in granular material to the development and functioning of brain. Besides the scaling properties of networks, their information-related properties are important. The amount of information contained by a network can be estimated by calculating its entropy, such as the Shannon entropy. This universal property is applicable to different types of networks from clusters of colloidal particles to cortical networks of neurons in the human brain.

The objectives of this study are:

- To study whether complex dependencies of blood flow velocity inside the system of vessel can be approximated by a simple allometric scaling relationship (*West et al, 1997*) with the help of CFD simulation.

- To analysis the mechanism which is contributing the ergodicity breaking in biophysical fluid transport system.

- To calculate the amount of information contained in networks, arising from small colloidal particles and droplet clusters (calculation of Shannon entropy)

- To investigate the applicability of two physical concepts: self-organizing criticality (SOC) and the percolation, relevant to the self-organization of neural networks.

- To find scaling relationship of cortical networks, which suggest that the characteristic time (rate of neural process) is independent of the brain size, when interspecies comparison is conducted.

In chapter 2, I will extend the allometric model to include micro/nano-fluidic capillary phenomena and investigate the ergodicity breaking caused by the fractal nature of the capillary branching model.

In chapter 3, I will concentrate on the ergodicity of the blood flow in the cardiovascular system. Then, I calculate the fraction of time that a blood cell (e.g. Red Blood Corpuscles) spends in a certain fraction of total volume of the vascular system and compare the temporal and volumetric fractions.

In chapter 4, scaling and dimensional analysis is applied to on networks, which contain fractal, scale-free and small-world properties. The quantity of information contained in a network could be estimated by the calculation of its Shannon entropy. Networks arising from tiny colloidal particles and droplet clusters due to pairwise interaction between the particles, have been considered in our work. In the colloidal science, due to influence of percolation and self-organized critically, networks have self-organizing properties and these properties tune the colloidal particles to the critical state, where system becomes unstable.

In chapter 5, discussion of much more complex networks such neurons, which are organized in neocortex, has been analyzed. Scaling relationship found in the neocortex suggests that characteristic time constant is independent of brain size when interspecies comparison is analyzed.

In chapter 6, two physical concepts such as self-organizing criticality (SOC) and percolation, relevant to the self-organization of neural networks have been demonstrated. *Sand-pile conceptual model* of SOC and hypotheses of brain network formation by SOC, have been analyzed. The role of percolation to trigger avalanche in a system has also been described.

In chapter 7, review of experimental data regarding the scaling properties of cortical networks related to their temporal and spatial orientation, has been reckoned. We extract the informational content of those cortical networks from entropic point of view. Scaling relationship of cortical networks suggest that characteristic time constant is independent of the brain size, when interspecies comparison is conducted.

To this end, we extrapolate the allometric model to include micro and nanofluidic capillary phenomena and investigate the ergodicity breaking caused by fractal nature of capillary branching model. We also analyze and review the application of networks to different areas, namely, to colloidal crystals and clusters and to networks of neurons connected by synapses. We discuss approaches to establishing scaling laws in these systems, investigating their dimensional and topological properties and using entropic methods to estimate information content.

2. Allometric law and ergodicity in vascular networks

In this chapter, we investigate scaling properties of vascular networks with fractal topology. This chapter is based on the paper [Nosonovsky M.; Roy P. Allometric scaling law and ergodicity breaking in the vascular system. *Microfluidics and Nanofluidic-Springer*. 2020.](#)

2.1. Formulation of the problem

Ergodicity or the equivalence of time and space averages is an important property of dynamical systems. Roughly speaking, ergodic systems have no memory of their previous history, and they tend to attain all microstates available. Contrary to that, non-ergodic systems demonstrate evolution with time or aging, which affects their ability to attain microstates with equal probability. The concept of ergodicity was first introduced by Ludwig Boltzmann, and it was further advanced in 1890 by Henri Poincaré's Recurrence Theorem stating that phase-space volume-preserving systems will always return to a state identical or very close to their initial state.

In biomedical fields, it is required to observe in vivo temporal evolution of various parameters. Sometimes, prolonged data acquisition is necessary, which is impractical indeed. Hence, understanding the ergodicity breaking mechanisms is significantly important to study bio-fluid (e.g. blood flow) transport system. Again, ergodicity is crucial for practical aspects of measuring parameters in a system, so prolonged observations of temporal behavior is often impossible and then, measurements should be substituted with finite time measurements (*Guzman-Sepulveda et al. 2017; Magdziarz and Zorawik 2019*). Ergodicity has myriad implications on aspects of behavior of dynamical system, such as its stability and quasi-periodic motion as well as to its qualitative

behavior (*Arnold 1968 & 1978*), for example, to identify Lagrangian Coherent Structures (LCSs) in fluid flow (*Rypina et al. 2011*).

One domain where ergodicity breaking is particularly important is biophysical transport of liquids including the hemodynamics (blood flow dynamics), intracellular and extracellular transport of complex media in biological systems including cytoplasm and nucleoplasm, macromolecular biopolymer solutions, and plasma cellular membranes (*Kulkarni et al. 2003; Földes-Papp and Baumann 2011; Manzo et al. 2015*). Ergodicity breaking in biological fluids is associated with macromolecular crowding which causes the anomalous diffusion deviating from the classical Einstein – von Smoluchowski model of mean-square displacement being a linear function of the lag time, $\langle r^2 \rangle \propto t$. Contrary to that, the anomalous diffusion results in the dependency which has the form of a power law

$$\langle r^2 \rangle \propto t^\alpha \tag{2.1}$$

with $\alpha < 1$ for the subdiffusion (which is the common case) (*Hofling and Franosch 2013*).

The allometric scaling relationships were summarized by the empirical Kleiber law. *Kleiber (1932, 1947)* compared metabolism rates, B , in various species and found that it is well approximated by a power-law scaling dependency on the mass of an animal, $B \propto M^{0.75}$. The value of the exponent, $a = 0.75$ remained mysterious until the seminal paper by *West et al. (1997)* explained it using the fractal model of branching of blood vessels serving a certain volume with the simultaneous conservation of the cross-sectional area of the vessels and of the volume covered at every stage of branching. Scaling methods and dimensional analysis are widely used in various areas of physics. One distinct fascinating implementation is biophysical problems, where both experimental observations and theoretical explanations have been suggested of how various quantitative characteristics of a living organism, for example rate of metabolism, depend on its mass and linear size. The area is often referred to as *allometry*.

2.2 Scaling relationships for a branching capillary system

Scaling relationships play traditionally a significant role in biophysics. Thus, scaling considerations define the size and properties of living cells (*Fabry et al. 2003; Bormashenko and Voronel 2018*). A particularly important area of biophysical scaling is the allometry or the quantitative study of the relationship of body size to living organism physiology.

2.2.1. Branching with area and volume conservation

West et al. (1997) suggested allometric scaling law for a branching cardiovascular network based on the assumptions of volume- and area-preserving branching. According to their analysis, when a tube with the length l_k and radius r_k branches into n tubes with the lengths $l_{k+1} = \gamma l_k$ and radii $r_{k+1} = \beta r_k$, the volume served by the next generation tubes and their cross-section area should conserve, which leads to the scaling relationships $\gamma \propto n^{-1/3}$ and $\beta \propto n^{-1/2}$. The volume is preserved because the same volume in the organism is served by blood vessels of different hierarchical levels. The area is preserved on the assumption of the constant rate of the fluid flow at different hierarchical levels (**Fig. 2.1**).

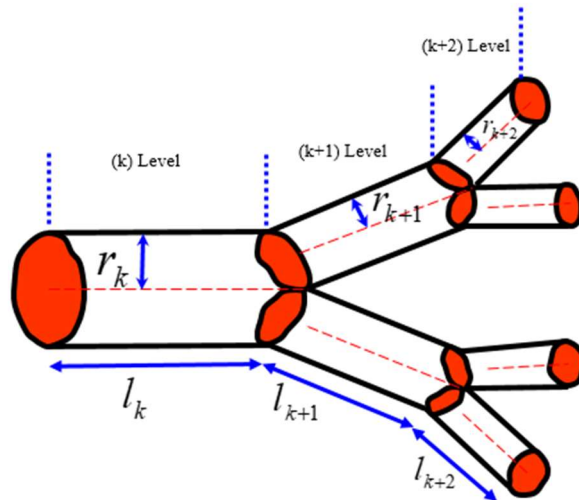


Figure 2.1. Branching of a vascular network; three levels are shown

The total volume of fluid is given by the sum of the geometric series $V = V_0 \frac{(\gamma\beta^2)^{-N}}{1-n\gamma\beta^2}$, where V_0 is a certain elementary volume (e.g., volume served by a capillary) and N is the total number of branch generations. Therefore, the volume scales as $V \propto (\gamma\beta^2)^{-N}$. From this, the scaling dependency of the total number of capillaries as a function of volume is $n^N \propto V^a \propto (\gamma\beta^2)^{-N} \propto (n^{-4/3})^{-N} \propto n^{4Na/3}$ yielding $a=3/4$, the well-established empirical results known as the Kleiber law.

The total volume of fluid in the cardiovascular network was further assumed to be linearly proportional to mass of the organism, while the number of capillaries is proportional to the flow rate and the rate of metabolic processes in general, leading to various conclusions, e.g., that the lifespan scales with the mass of an animal as $M^{1/4}$ (Bejan 2012).

2.1.2. Considering more realistic scaling dependencies

Note that the branching model by *West et al. (1997)* does not take into account neither the physico-chemical capillary effects due to the interfacial tension of the liquids, nor the tortuosity of the capillaries. Human blood is a non-Newtonian multi-component fluid consisting of the liquid plasma (55% of total blood volume formed 95% of water with various dissolved substances), red blood cells or erythrocytes (flexible disks of the 6-8 μm diameter), white blood cells or leucocytes of different types (diameter of 7-30 μm) and platelets (2-3 μm diameter). The radius of blood vessels varies by about 3000 times from 15 mm in the aorta to 5 μm in the capillaries, while the flow velocity changes by about 1300 times from 0.4 m/s in the aorta to 0.3 mm/s in the capillaries. This is in striking contradiction with the assumption of constant rate of the fluid flow at different hierarchical levels.

Computation Fluid Dynamics (CFD) simulations demonstrate that even simple branching (bifurcation, $n=2$) of a vessels results in a complex flow velocity profile. Thus **Fig. 2.2** shows CFD modeling results for bifurcation of a blood vessel for typical blood flow conditions at the peak systolic phase. The velocity profile and flow streamlines are far from being uniform. Therefore, the scaling assumption for velocities in a branching network can be satisfied only approximately.

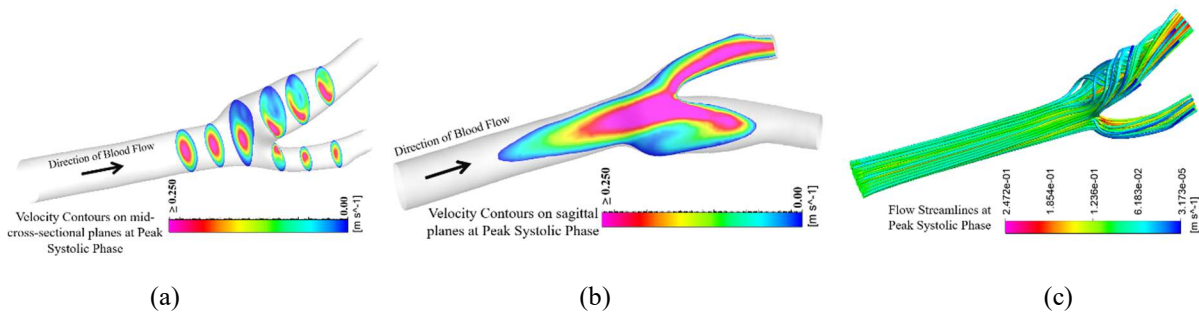


Figure 2.2. CFD simulation of blood flow through a bifurcating (branching) vessel shows complex dependencies of velocity, which cannot be approximated by a simple scaling relationship. Velocity contours in (a) perpendicular and (b) parallel cross-section and (c) flow streamlines for the peak systolic phase are shown.

The surface tension of blood is rarely discussed in biomedical literature, although it is significantly lower than that of water (about 56 mN/m at room temperature, while water surface tension is about 72 mN/m) and it has been associated with the genesis decompression sickness and other processes in the organism (*Hrnčír and Rosina, 1997; Krishnan et al., 2005*). The intensive study of the superhydrophobicity (surface roughness-induced non-wetting) brought the idea of surface roughness induced self-cleaning in the liquid flow including the oleophobicity (repelling organic liquids such as oils), underwater oleophobicity to reduce fouling, and the shark skin effect (flow drag reduction due to specially oriented micro-riblets). Maani et al. (2015) suggested the micro/nanostructure-controlled adhesion in blood flow for cardiovascular applications, where it is desirable to reduce stagnation and clotting of blood. Complex structure of blood vessel surface layers along with a complex multiphase composition of blood may result in significant surface-induced effects (**Fig. 2.3**) Biomedical “hemophobic” applications can prevent blood clotting and thrombosis by controlling the surface pattern at a wall of a catheter or stent (Ramachandran et al., 2015). Taking into account the surface effect may modify the of cross-sectional area preservation for small capillaries, leading to $\beta \propto n^{-1}$.

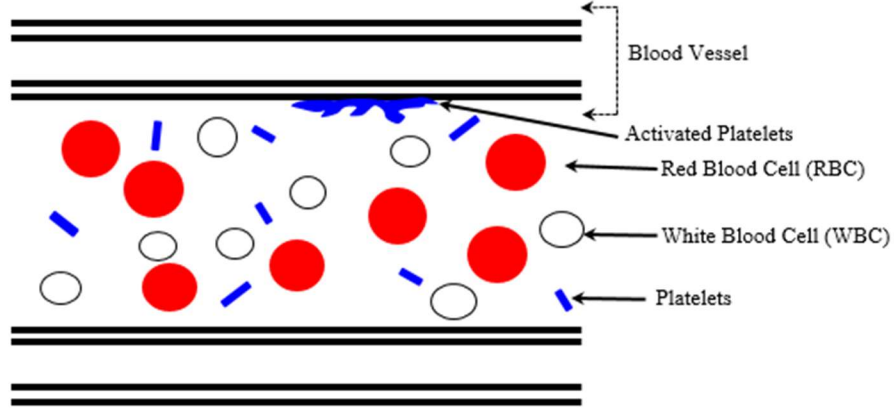


Figure 2.3. Schematic of blood flow in a blood vessel showing layers of the blood vessel and various components of blood. The interaction with the blood vessel wall is important due to its medical significance and hemodynamic effects (*Maani et al.* 2015).

Due to the liquid volume preservation postulate, $\pi r_k^2 u_k = n \pi r_{k+1}^2 u_{k+1}$, the velocity scales as $\frac{u_k}{u_{k+1}} = n \frac{r_{k+1}^2}{r_k^2} = n \beta^2$. Under the assumption of cross-sectional area preservation, $\beta \propto n^{-1/2}$, this leads to a constant value of the flow velocity in the system, $u_k = u$; however, experimental data indicate that the flow velocity may be different at different branching levels. The decrease of the flow speed roughly by the same order as vessel radius scales well with the assumption of $\beta \propto n^{-1/3}$

The total time spent by a particle or molecule at the k -th level is given by

$$\frac{T_{k+1}}{T_k} = \frac{l_{k+1} u_k}{u_{k+1} l_k} = \gamma n \beta^2 = n^{1-b-2c} \quad (2.2)$$

To accommodate for the vascular resistance, the Hagen–Poiseuille equation is often used, which states that the resistance to the blood flow scales as r^{-4} or the *Thurston (1976)* equation, which scales the flow resistance as r^{-3} . There are different ways to account for the size effect due to the capillary effects, however, in general the assumption of the dependencies of γ and β on n should be modified.

In addition, capillaries are not straight tubes. The effect of capillary tortuosity of curvature can be scale-dependent. To account for all these effects, we can consider more general scaling relationships $\gamma \propto n^{-b}$ and $\beta \propto n^{-c}$ would lead to the power exponent

$$a = 1/(b + 2c) \quad (2.3)$$

This relationship is based on the fractal geometry of branching vessels. In the following chapter we will discuss ergodicity of the fractal scaling model presented here.

3. Ergodicity breaking analysis

In the preceding chapter we develop a scaling model for a vascular network. In this chapter, let us now concentrate on the ergodicity of the blood flow in the vascular system. For that end, we will calculate the fraction of time that a blood cell spends in a certain fraction of the total volume of the circularly system and will compare the temporal and volumetric fractions.

The total time that a blood particle (including cells or molecules) spends in the circulatory system is given by the sum of the series

$$T = \sum_{k=1}^{\infty} T_k = \sum_{k=1}^{\infty} \frac{l_k}{u_k} = \frac{l_1}{u_1(1-n^{1-b-2c})} \quad (3.1)$$

where l_1 is the length of the highest hierarchical level. For $b=1/3$ and $c=1/2$, **Eq. 3.1** yields $T = \frac{l_1}{u(1-1/\sqrt[3]{n})}$.

Let us calculate the time, which a blood particle spends at the levels of the system starting from $k = m$ to $k = \infty$ using the formula of a partial sum of a geometric series. The assumption behind this calculation is that only blood vessels $k = m, \dots, \infty$ serve the volume defined by the length l_k (the volume itself is given by the sphere $32\pi l_m^3/3$). Consequently, the ratio of the time spent at the levels starting $k = m, \dots, \infty$ to the total time in the vascular system, T , is given by the time fraction

$$\theta_m = \left(\frac{T_{k+1}}{T_k}\right)^{m-1} = n^{(1-b-2c)(m-1)} \quad (3.2)$$

Note that for $b=1/3$ and $c=1/2$, **Eq. 3.2** yields $\theta_m = n^{-(m-1)/3}$.

Consider a region with the radius $R = 2l_m$ and volume $32\pi l_m^3/3$. This volume constitutes the fraction of the total volume

$$\rho_m = \frac{l_m^3}{l_1^3} = \gamma^{3(m-1)} = n^{-3b(m-1)} \quad (3.3)$$

The volume distribution of the capillaries is uniform, therefore, the probability to find a liquid molecule or cell/particle in a given volume is supplied by ρ_m . On the other hand, the time fraction spent by a single blood cell or molecule at a given volume $32\pi l_m^3/3$ is given by θ_m , and

thus the ratio of the probability to find a single cell or molecule within a certain volume during its motion to the fraction of molecules in this volume is

$$\frac{\theta_m}{\rho_m} = \frac{n^{(1-b-2c)(m-1)}}{n^{-3b(m-1)}} = n^{(1+2b-2c)(m-1)} \quad (3.4)$$

In general, the ratio supplied by **Eq. 3.4** is dependent on m , and, therefore, it is dependent on the size of the volume thus indicating that the motion is not ergodic. Due to the fractal nature of the capillary system, a particle tends to spend much more time in smaller volumes in comparison to the volume fracture. Note that for $b=1/3$ and $c=1/2$, **Eq. 3.4** yields

$$\frac{\theta_m}{\rho_m} = n^{2(m-1)/3} \quad (3.5)$$

Using $3b(m-1)\ln n = -\ln \rho_m$ we find $m-1 = -\ln \rho_m / (3b \ln n)$. By further substituting the value of m into **Eq. 3.4** and finding a logarithm, we obtain

$$\ln \theta_m = \frac{b-1+2c}{3b} \ln \rho_m + \ln(n^{-1+b+2c}) \quad (3.6)$$

The number of the hierarchical level m is eliminated from **Eq. 3.6**, which presents the dependency of the time fraction spent in a certain volume upon its volume fraction of the total volume. By interpolating it, one finds the dependency of the probability for a particle to be found in a certain volume based on the time spend there to the probability to find a particle in that volume based on the volume fraction

$$\theta = \rho^{\frac{b-1+2c}{3b}} \quad (3.7)$$

For a given volume, the space-average probability to find a particle is proportional to that volume. Note that the volume of the organ and the liquid volume of the blood vessel system serving that volume are two different volumes. We use the first one for the calculation of space-averaged probability.

Three dependencies of the time fraction spent in a certain volume upon its volume fraction, $\theta(\rho)$, are shown in **Fig. 3.1(a)** for different values of a and b . Note that for $b=1/3$ and $c=1/2$, **Eq. 3.7** yields a non-linear (and, therefore, non-ergodic) dependency $\theta = \sqrt[3]{\rho}$.

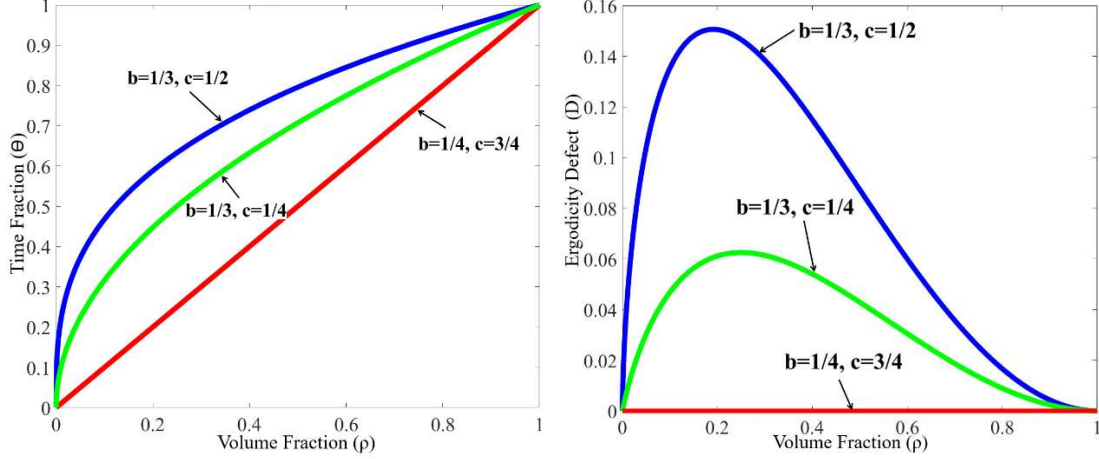


Fig. 3.1. (a) Time fraction and (b) ergodicity defect as a function of the volume fraction for three combinations of parameters a and b .

The ergodicity condition would imply equal time spent in equal volumes and, therefore, a linear dependency between corresponding variables, $\theta \sim \rho$. This is achieved when the following ergodicity condition is satisfied

$$b = c - \frac{1}{2} \quad (3.8)$$

For example, in Fig. 4(a) the linear dependency for $b = 1/4, c = 3/4$ is the ergodic case. Combining **Eqs. 2.3 and 3.8** gives $a = 2/(6c - 1)$. For volume-preserving branching, $b=1/3$, this yields $c = 5/6$ and $a = 1/2$. This is inconsistent with the Kleiber law, which relates the metabolic rates the animal mass, $B \propto M^a$ as $a=3/4$. On the other hand, the Kleiber law, $a=3/4$, is satisfied when $b = 25/22 \approx 1.136$ and $c = 18/11 \approx 1.636$ which contradicts the volume-preserving branching assumption. We conclude that for the realistic situations (the volume-preserving branching and the Kleiber law) the model predicts non-ergodic behavior.

The calculation demonstrates that flow systems with fractal branching exhibit non-ergodic behavior. Such systems including vascular networks tend to be fractal because they involve the flow through a 2D cross-section, which covers a 3D volume delivering fluid to the vicinity of every point of the volume (every cell) with equal probability. In addition to covering the volume with equal probability, they should supply the fluid continuously in the temporal domain. However, due to the fractal organization of the vascular network, the flow “decelerates” at small length scales. Consequently, particles (including molecules and cells) spend more time at small volumes, in

comparison with the volumetric fraction of these volumes. We interpret this feature of fractal behavior as ergodicity breaking.

While more traditional sources of ergodicity breaking in biophysical fluid transport systems include time evolution or aging of the particles and macromolecular crowding, it is not uncommon that fractal geometry of a trajectory results in an effective deceleration of motion. One example would be the “hydrodynamic memory” which slows down the diffusion (*Hofling and Franosch 2013*). Another example is the so called “dissipative anomaly” in the turbulent flow, when the dissipation does not approach zero even at the zero-viscosity limit, so that fractal trajectories lead to deceleration (*De Lellis and Székelyhidi 2019; Shnirelman 2000*).

Several measures of deviation from the ergodic behavior have been suggested in the literature. Földes-Papp and Baumann (2011) suggested decoupling the effects of the molecular crowding and the temporal heterogeneity by presenting the power exponent, which controls the dynamics of the interaction network, as a product of these two factors.

Scott et al. (2009) suggested the ergodicity defect D , defined at different scales (on a map T) with respect to a function f given by an integral of the square of the space and time averages $D(f, T) \propto \int (f^*(x, T) - \bar{f})^2 dx$, where f^* and \bar{f} are the time and space averages. The ergodicity defect defined in this manner can be used to identify the structure of the solution, such as the LCS (*Rypina et al. 2011*). Using **Eq. 3.7**, one can suggest

$$D = (\theta - \rho)^2 = \rho^2 \left(\rho^{\frac{-2b-1+2c}{3b}} - 1 \right)^2 \quad (3.9)$$

Fig. 3.1b shows a plot of the ergodicity defect vs. the volume fraction for the values of the parameters used in **Fig. 3.1a**.

Ergodicity breaking due to scale-dependent behavior is also significant for small systems of colloidal or droplet clusters. These systems are used for *in situ* tracking of biomolecules and bioaerosols (*Fedorets et al. 2019a*). *Lim et al. (2019)* reported the transitions from sticky to ergodic configurations in six-particle and seven-particle systems of hard spheres. *Fedorets et al. (2019b)* studied small oscillations of a microdroplet cluster levitating in an ascending vapor stream and found that the cluster tends to oscillate as a whole. They showed that the synchronization of droplets’ trajectories is not caused by the interactions between them, but by external fluctuations with the characteristic length scale much larger than the size of the droplets. In this case, the center of mass of the entire cluster produces the same motion as single micro-droplets, indicating ergodic

behavior. Ergodicity breaking in this case is related to the scale ratio of the external fluctuation and the system.

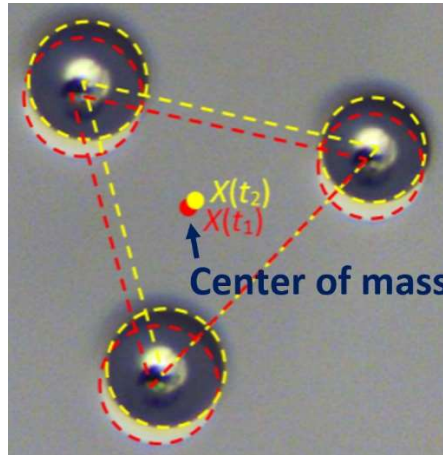


Figure 3.2. Oscillations of a small levitating droplet cluster, which vibrates as a whole (*Fedorets et al. 2019b*)

Understanding the ergodicity breaking in fluid flow of branching vascular network is also relevant to micro/nanofluidic applications, such as the artificial biomimetic vascularized tissues. Such tissues are being developed for both medical applications of tissue engineered constructs (*Hasan et al. 2014*) and for such applications as self-healing materials where a flow of liquid agent is required (*Nosonovsky and Rohatgi 2012*).

4. Clusters and Networks

In the preceding chapters we discuss scaling in vascular networks based on fractal flow branching. Starting from this chapter, the thesis will review networks in materials science and neural networks. Chapters 4 to 7 are based on [Nosonovsky M.; Roy P. Scaling and Entropy in colloidal and neural networks. *Entropy-MPDI*. 2020.](#)

4.1. *Networks in Material Science*

Let us start from the discussion of clusters. Cluster is defined as collections of somewhat similar, but not necessarily identical objects. In physics and chemistry, clusters are often built of liquid droplets or small solid particles, such as nanoparticles, and colloidal particles (*Bormashenko et al., 2020*). Clusters often possess interesting properties because, from the physical point of view, they occupy an intermediate position between individual objects and bulk material consisting of a large number of objects, to which the methods of statistical physics and thermodynamics are often applied. Since clusters bridge between individual particles and bulk matter, they may have certain unique collective properties absent in both individual objects and in bulk materials.

Given that there are interactions between particles in a cluster, the latter can be modeled by a network. A network is a graph, which consists of nodes (vertices) connected by edges. Topology and scaling behavior of various networks has been studied extensively since the 1990s. A number of important properties have been discovered experimentally in real life networks including the scale-free and small-world network behavior.

The number of connections of a given node in a network with other nodes is called the *degree* of the node, k . The probability distribution function of the degree of the node in the entire network is called the *degree distribution*, $P(k)$. An important class of large networks have the degree distribution functions, which approximately follow a power law

$$P(k) \propto k^{-a}. \quad (4.1)$$

where a is a constant, typically in the range $2 < a < 3$. Such a network is called a “scale-free” network. For $a < 3$, the standard deviation of the degree diverges, and the network lacks a characteristic degree; hence the name a “scale-free network”.

Scale-free networks are abundant in nature and culture including various biological, social, and technical systems, such diverse as citation and co-author scientific networks, the internet, and protein-protein interaction (*Albert and Barabási 2002*). The commonly used algorithm to create a scale-free network is the *Barabási and Albert (1999)* model (BA model). The BA model is often compared with the random graph *Erdős–Rényi (1959)* (ER) model of a random network. Unlike a scale-free network, the random ER network has the average degree value, k_{ave} .

Scale-free behavior is common not only in networks. It emerges in various areas of physics and it is associated with the fractal phenomena and with the near-critical behavior close to the

phase transition. Many scale-free systems are governed by so-called self-organized criticality, whose characteristic signature is the one-over-frequency noise and avalanche-like behavior.

Scale-free networks have some nodes with a degree that greatly exceeds the average, and such highly connected nodes are called “hubs.” In real-life networks hubs often have specificity, for example, they can connect parts of a network; in social networks hubs may correspond to “celebrities,” etc. Smaller hubs are present next to major hubs thus creating a hierarchical organizational structure of a scale-free network. Scale free networks have high resilience or tolerance towards failure. If a number of nodes, including hubs, are removed from the network, it still remains connected.

Quantitatively, the resilience is characterized by the critical percolation threshold, p_c , or the fraction of nodes which should be kept to sustain the connectivity. Thus, for an infinite network with $2 < a < 3$, the critical percolation is zero, $p_c = 0$, which means that removing randomly any fraction of the network cannot destroy it. For finite scale-free network with N nodes, $p_c \sim N^{1/3}$; thus a large network such as the Internet with $N > 10^9$ will not be destroyed until more than 99.9% of nodes are removed in a random manner (however, it can be destroyed if high-degree nodes are removed preferentially). Note that, as opposed to the scale-free network, in a ER random network, the threshold percolation is non zero, and it is inversely proportional to the average degree $p_c \sim 1/k_{ave}$.

A path or a walk within a network is a sequence of incident nodes and edges. Nodes or edges can appear in the same path more than once. The geodesic path is the shortest path between any two nodes, whereas the geodesic distance between two nodes is the minimum number of edges connecting these two nodes or the shortest path length between them. A network is considered “small world” if a typical geodesic distance between two randomly chosen nodes is proportional to the logarithm of the total number of nodes in the network

$$L \propto \log (N). \tag{4.2}$$

The small-world concept implies that despite their large size, in most networks, there is a relatively short path between any two nodes (**Fig. 4.1**). The commonly studied type of the small-world networks is the *Watts and Strogatz (1998)* model.

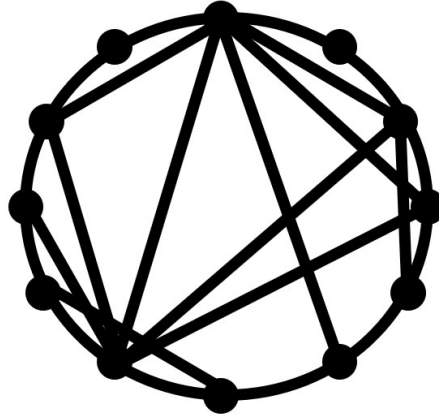


Figure 4.1. Small world network concept. While some nodes have connections only with their neighbors, edges connecting with remote nodes provide short geodesic paths

The clustering coefficient is defined as a ratio of the number of closed triplets to all triplets. This coefficient is a measure of the degree to which nodes in a graph tend to cluster together. It is used to quantify aggregation in granular media indicating the degree of clustering of particles in the cluster.

The topological concepts from the theory of networks turn out to be useful for physical characterization of packing of granular material, colloidal crystals, and clusters of droplets and colloidal particles.

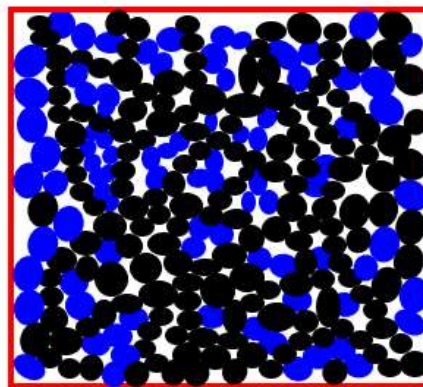


Fig. 4.2. Model of jamming in a granular media as percolation of a force network. The force is transmitted through chains of connecting grains shown in black. (*Majumdar and Behringer, 2005; Gendelman et al., 2017*).

The so-called *force network* is important for the understanding of packing of granular material (**Fig. 4.2**). The force network connects centers of mass of each pair of grains that have a force transmitting contact. Such network presentation provides key insights for understanding the mechanical response of a soil or sand heap. Moreover, percolation, i.e., the formation of a force-transmitting chain in such network corresponds to the jamming transition in the granular material (*Majumdar and Behringer, 2005; Gendelman et al.*). The percolation phenomenon in application to networks will be discussed more in detail in the consequent section.

In particular, the small-world effect and scale-free behavior were reported for packing problems related to aggregation of granular media which employs the so-called “Apollonian packing” (*Andrade et al. 2005*). For simple packing of identical (monodisperse) particles, the force networks do not possess self-similar, scale-free, or small-world properties. However, to achieve high packing densities the Apollonian construction can be employed (**Fig. 4.3**). Such construction involves multiscale set of circles with smaller circles fitting the space between larger ones. This may be needed for high performance concrete (HPC) and certain ultra-strong ceramics. *Andrade et al. (2005)* found that the force networks resulting from the Apollonian construction, which they called Apollonian networks (ANs), have many special properties including the scale-free and small-world effects.

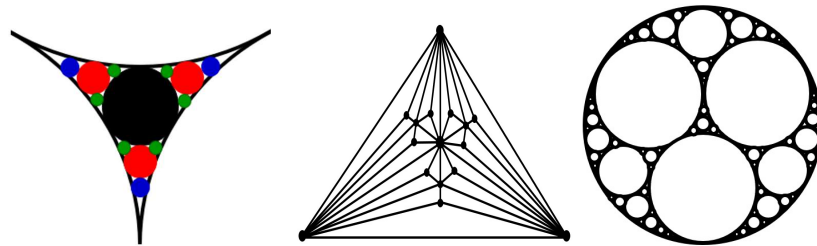


Figure 4.3. Apollonian packing and a corresponding graph (*Andrade et al., 2005*)

4.2. Droplets and clusters as networks

An even more interesting phenomena where the theory of networks can be applied are small droplet clusters (*Fedorets et al., 2017; Aktaev et al., 2018*) and small colloidal crystals. Self-assembled clusters of condensed microdroplets (with the typical diameter of dozens of microns) are formed in an ascending stream of vapor and air above a locally heated thin (~ 1 mm) layer of water. The droplets form a 2D monolayer levitating at a low height (comparable with their radii)

where their weight is equilibrated by the drag force from the ascending vapor flow. Due to an aerodynamic interaction (repulsion) between the droplets and their migration towards the center of the heated spot, they tend to form an ordered structure (**Fig. 4.4**).

For large clusters consisting of many dozens or hundreds of droplets, a hexagonally symmetric (honeycomb) structure is typically formed. However, for small clusters more complex symmetric structures can form. Small clusters can be used for *in situ* tracking of bioaerosols and biomolecules (*Fedorets et al. 2019; Bormashenko et al, 2019*)

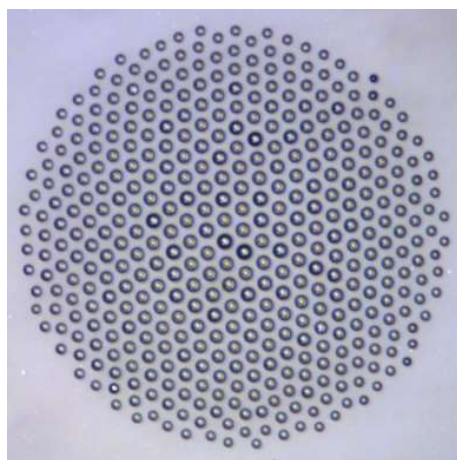


Fig. 4.4. A hexagonally ordered 2D droplet cluster levitating over a water surface. The size of the frame is 0.75 mm (*Bormashenko et al., 2019-Entropy paper*).

Unlike liquid water droplets, colloidal particles are solids and they can form small clusters, which can levitate due to acoustic waves or another mechanism, but they form a closed packed structure. Thus, *Perry et al. (2015)* studied the structural rearrangement in a 2D levitating of cluster of solid *sulfate polystyrene* spherical particles. Individual particles in a particular configuration (an excited state) of the cluster may have bonds between them. For a system of six particles, *Perry et al. (2015)* identified a number of seven-bond and eight-bond configurations. Similar systems. *Lim et al. (2019)* reported the transitions from sticky to ergodic configurations in six-particle and seven-particle systems of hard 1.3 μm diameter spheres (**Fig. 4.5**). The six-particle system can form various arrangements, with different probabilities of these arrangements.

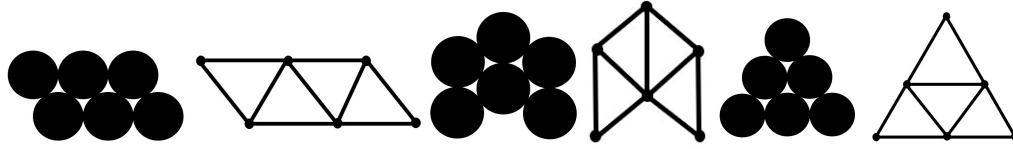


Fig. 4.5. Schematic of colloidal particles forming small clusters (based on *Perry et al., 2015*)

For many distributions of small elements (for example, the words in a language or letters in a text), an empirical power law, such as the Zipf law, is found. The Zipf law is given by the formula

$$P(k) = \frac{k^{-a}}{\sum_{n=1}^N n^{-a}} \quad (4.3)$$

where the denominator is needed for normalization. A power law distribution may be expected for the probabilities of various excited states forming a set of rearrangement configurations. It is instructive to investigate the probabilistic distributions and information content in graphs corresponding to small clusters.

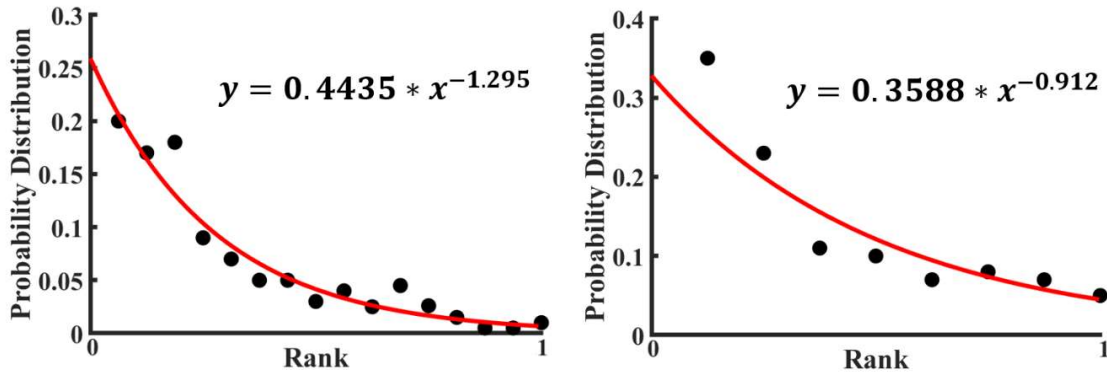


Figure 4.6. Experimental probability distributions of 8-bonds (right part) and 7-bonds (left part) structures. Each point is representing each distinguished structure of colloidal cluster. (based on *Perry et. al, 2015*).

For the data by Perry et al. (2015), the probability distribution of various configurations was plotted in **Fig. 4.6**. A calculation based on the empirical formulae of the Zipf Law (**Eq. 4.3**) using the experimental data points has been done to fit those experimental points. Then, a fitted curve also has been plotted in **Fig. 4.6** with the data presented also in **Table 4.1**. The value of the power exponent in the curve fitting equation is almost unity which indicates the fitted curve is

hyperbolic in nature. Simultaneously, this Zipf-Law distribution curve features each distinguished structures of colloidal clusters lie in the scale-free network system.

The information content of a distribution is characterized by the Shannon entropy, which is given by

$$S = -\sum_{n=1}^N p_n \log_2 (p_n). \quad (4.4)$$

where p_n is the statistical probability of the n -th state and N is the total number of states. The Shannon entropy is used in materials science, for example, as a surface roughness parameter characterizing informational content in the surface given by its profile (*Nosonovsky and Mortazavi, 2014*). The Shannon-entropy-based informational approach is also used for various other aspects of the surface science, such as wetting transitions (*Nosonovsky, 2018*) and stick-slip transition (*Nosonovsky and Breki, 2019*).

Using the data from **Fig. 4.6** and **Table 4.1 and 4.2**, the following values were obtained. For the seven-bond configurations, the value of the Shannon entropy $S=2.745$ was obtained, while for the eight-bond configuration, the value of $S=3.400$ was obtained. The Shannon entropy provides an estimation of the information content in these configurations. The values of Shannon entropy characterizing the information content of the colloidal cluster system will be later related to information content of other networks.

To conclude this section, methods of the network science can be used for the analysis of various systems studied by the physical chemistry and materials science. These include granular materials, colloidal crystals and clusters made of small particles or droplets. Many of such systems form sets of configurations, somewhat similar to the set of symbols (e.g., letters) and characterized by power-law statistical distributions typical for the latter. The power law distribution is also characteristic for scale-free networks, which will be discussed more in detail in the following chapter. The information content of these structures can be estimated using the Shannon entropy approach.

Table 4.1. Structures of 7-bonds colloidal clusters and their magnitudes of probability distribution and Zipf-Law distribution (*Perry et al, 2015*)

























	A	B	C	D	E	F	G	H
Structures								
Probability	0.35±0.1	0.23±0.06	0.11±0.05	0.10±0.02	0.07±0.01	0.08±0.02	0.07±0.01	0.05±0.0
Zipf-Law	0.36	0.19	0.14	0.10	0.08	0.07	0.06	0.05

Table 4.2. Structures of 8-bonds colloidal clusters and their magnitudes of probability distribution and Zipf-Law distribution (*Perry et al, 2015*)

	A	B	C	D	E	F	G	H
Structure								
Probability	0.20±0.05	0.17±0.03	0.18±0.03	0.09±0.03	0.07±0.01	0.05±0.01	0.05±0.02	0.03±0.001
Zipf-Law	0.21	0.16	0.14	0.10	0.09	0.07	0.05	0.04
	I	J	K	L	M	N	O	P
Structures								
Probability	0.04±0.002	0.025±0.002	0.045±0.002	0.026±0.002	0.015±0.001	0.005±0.0	0.005±0.0	0.01±0.001
Zipf-Law	0.03	0.02	0.02	0.02	0.01	0.007	0.007	0.01

5. Multiscale organization of neo-cortex network

In the previous chapter we discussed colloidal networks relevant to the materials science. Here we will concentrate on organization of neocortex and quantitative estimation of the brain network characteristics.

5.1. Organization of neo-cortex: macro-columns and mini-columns

Various aspects of scaling behavior have been studied for networks associated with brain. Neuron connections in human brain constitute a very complex network of about 10^{10} neurons with more than 10^{14} synapses connecting between them. While it is extremely difficult to study such a complex network, a number of important insights have been achieved, particularly, since the early 2000s. This knowledge was obtained due to novel methods of *in vivo* observation of neural activity, including the electroencephalography (EEG), functional magnetic resonance imaging (fMRI), diffusion tensor imaging (DTI), two-photon excitation microscopy (TPEF or 2PEF), and positron emission tomography (PET).

Many insights were also achieved using the comparison or analogy of the human brain with much simpler organisms, such as the nematode *Caenorhabditis elegans* (a tiny worm with the size of less than 1 mm), which has only 302 neurons and about 6398 synapses. Since a complete connectome (a map of neuron connections) and genome have been obtained and published for *C. elegans*, this worm serves as a model organism for genetic and neurological research.

As far as the human brain, the higher order brain functions, such as cognition, language, sensory perception, and generation of motor commands are associated with the neocortex. The neocortex is an external part of the brain, which is 3-4 mm thick and with the surface area of 0.26 m². The neocortex is made of six distinct layers of neurons and it consists of 10^8 cortical mini-columns with the diameter of about 50-60 μm spanning through all six layers, with about 100 neurons in each mini-column (**Fig. 5.1**). Although the functionality of the microcolumns (and their very existence) is being debated by some researchers, the columnar structure of the neocortex is widely accepted by most neuro-scientists. The microcolumns are combined into the large hyper-columns or macro-columns, 300-500 μm in diameter. The hyper-columns have a roughly

hexagonal shape, and each column is surrounded by six other columns. Each hyper-column, by some estimates, may include 60-80 microcolumns (*Mountcastle, 1997*).

While little is known about the processes inside the microcolumns, it is widely believed that a cortical column can process a number of inputs and it converts them to a number of outputs using overlapping internal processing chains. Each minicolumn is a complex local network that contains elements for redundancy and plasticity. The minicolumn unites vertical and horizontal cortical components, and its design has evolved specifically in the neocortex. Although minicolumns are often considered highly repetitive clone-like units, they display considerable heterogeneity between cortex areas and sometimes even within a given macrocolumn (*Buxhoeveden and Casanova, 2002*).

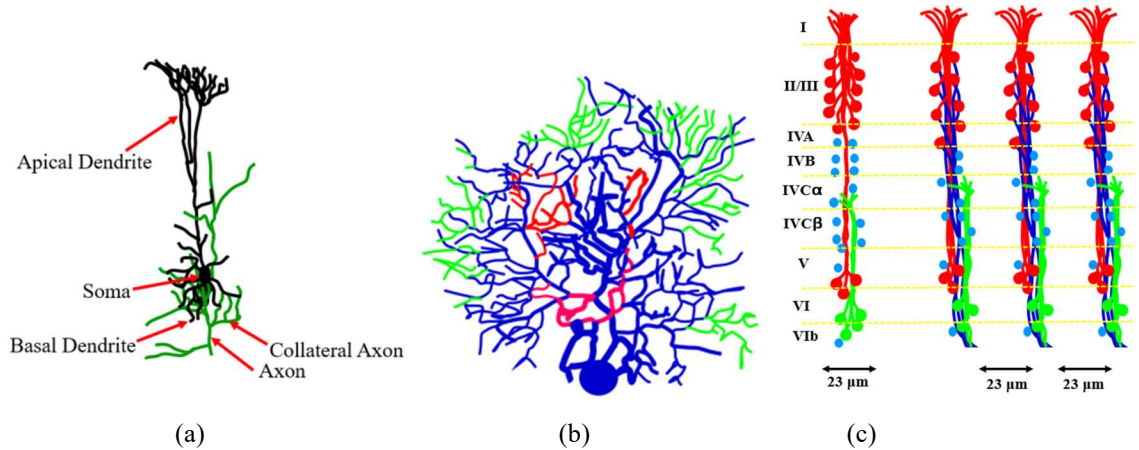


Figure 5.1. Neurons and their parts forming a network. (a) The arrangement of neurons, dendrites and axons in vertical modules of the striate cortex of the macaque monkey. (b) The arrangement of the apical dendrites of pyramidal cells in the cortex showing the six layers (I to VI). The cells in layers II to V (red), VI (green), and (IV) (blue, no dendrites) are shown. (c) Columns built of dendrites and axons. (based on *Mountcastle 1997*).

5.2. *Small-world and scale-invariant behavior*

A comprehensive map of neural connections in the brain is called the *connectome*. A connectome of the *C. elegans* worm has been obtained in the 1990s, while obtaining human brain connectome remains a much more challenging task of the scientific discipline referred to as *connectomics* (compare with genome and genomics or proteome and proteomics). A much more complex connectome of the *Drosophila melanogaster* fruit fly, a model insect used for various genetic research, whose brain contains about 135,000 neurons and 10^7 synapses, has been presumably obtained by 2020 (*Xu et al., 2020*).

It is believed that human connectome can be studied at three distinct levels of structural organization: the microscale (connection of single neurons), mesoscale (cortical columns), and the macroscale (anatomical regions of interest in the brain).

An amazing feature of brain operations is that they are distributed, rather than localized at a particular neuron or a group of neurons. The distributed operations are performed by a collection of processing units that are spatially separate and communicate by exchanging messages. Mountcastle (1997) formulated the following properties of such distributed systems

- Signals from one location to another may follow any of a number of pathways in the system. This provides the redundancy and resilience.
- Actions may be initiated at various nodal loci within a distributed system rather than at one particular spot.
- Local lesions within a distributed system usually may degrade a function, but not eliminate it completely.
- The nodes are open to both externally induced and internally generated signals.

Several neuro-scientists suggested in the 2000s that the human brain network is both scale-free and small-world, although the arguments and evidence for these hypotheses are indirect. Evidence of scale-free brain dynamics includes form, function, and spatiotemporal discontinuities, with such semi-empirical observations as power-law distributions of anatomical connectivity and their slow changes and of functional parameters of neural activity as well as the statistical properties of state transitions in brain (Freeman, 2006). These properties are similar to those of self-organized criticality (SOC) systems (i.e., similar to the famous sand-pile model, which will

be discussed in the next section) and they are characterized by the avalanche dynamics, one-over-frequency noise and fractal scale-free behavior as well as near-critical universal behavior.

Self-organizing critical behavior was reported by Liu et al. (2020) for the organization of brain GABAA receptors. The mean size of receptor networks in a synapse followed a power-law distribution as a function of receptor concentration with the exponent 1.87 representing the fractal dimension of receptor networks. The results suggested that receptor networks tend to attract more receptors to grow into larger networks in a manner typical for SOC systems which self-organize near critical states.

Freeman and Breakspear (2007) suggested that if neocortical connectivity and dynamics are scale-free, hubs should exist for most cognitive functions, where activity and connections are at maximum. These hubs organize brain functions at the microscopic and mesoscopic level. They are detectable by macroscopic imaging techniques such as fMRI. Therefore, these are hubs rather than localized functions, which are revealed by these imaging techniques.

Above a certain threshold of connection density, a scale-free network can undergo an abrupt avalanche-like state transition and resynchronization globally and almost instantaneously no matter how large its diameter. Scale-free dynamics can explain how mammalian brains operate on the same time scales despite differences in size ranging to 10^4 (mouse to whale). Random removals of nodes from scale-free networks have negligible effects, however, lesions of hubs are catastrophic. Examples in humans are coma and Parkinson's disease from small brain stem lesions.

Quantitative estimates of the brain network characteristics are remarkable. Bollobás and Riordan (2002) derived a measure of the diameter of the scale-free network of n nodes, which is given by $D = \log(n) / \log(\log n)$. The neocortical diameter can be calculated for each hemisphere by the number of neurons (0.5×10^{10}) and the number of synapses per neuron (10^4), yielding $n = 5 \times 10^{13}$ and a diameter of 12. These numbers significantly exceed those addressed by random graph theorists, suggesting that at least a three-level hierarchy should exist, formed by nodes as neurons (treating multiple possible synapses between any neuron pair as one edge), hypercolumns, and modules. The reduction of 10^{10} neurons and 10^{14} synapses to a depth of three levels and a diameter of $D=12$ underscores the simplification offered by random network theory for describing hemispheric-wide cortical dynamics.

Klimm et al. (2014) estimated quantitative characteristics of the human brain network including the hierarchy of the network and its fractal topological dimension. The hierarchy of a network, β ,

is defined quantitatively by the presumed power law relationship between the node degree and the local clustering coefficient (the ratio of the triangle subgraphs to the number of node triples), $C_i \sim k_i^{-\beta}$. The fractal dimension, d , is a measure of the network's complexity and is determined by the box-counting method relating the number of boxes N_B of size l_B that are necessary to cover the network, $N_B \sim l_N^{-d}$. They estimated $\beta=0.247$ and $d=3.7 \pm 0.1$.

6. Percolation and critically studies

In this chapter, two physical concepts i.e. (a) self-organizing criticality (SOC) and (b) percolation, relevant to the self-organization of neural networks have been explained. Then, sand-pile conceptual model of SOC and hypotheses of brain network formation by SOC, have been analyzed. The role of percolation to trigger avalanche in a system has been stated.

6.1. Percolation in materials and in networks

Two physical concepts relevant to the self-organization of neural networks are self-organized criticality (SOC) and percolation. As far as SOC, there is a big class of dynamical systems that operate in such a manner that they always tune themselves to the critical state, where the stability of the system is lost. Since the 1980s, it has been suggested that a very specific type of self-organization, called SOC, plays a role in diverse “avalanche-like” processes. Typically, energy is accumulated in these systems until the critical state is reached, and then energy is suddenly released. Examples are various avalanche systems, including those describing landslides, earthquakes and frictional stick-slip. A random perturbation can trigger an avalanche (or a slip event) in such a system. The magnitude of the avalanche cannot be predicted in advance, because

it is random. After the release, the system returns to the stable state for some time until the next event is triggered. The amplitudes of the events have statistical characteristics of critical behavior, such as universality, critical exponents and fractality.

The famous example is the power law which relates the frequency and the magnitude of earthquakes, known as the Gutenberg-Richter law. Similar behavior is observed, for example, in frictional stick-slip systems and in many other systems (*Nosonovsky and Mortazavi, 2014*).

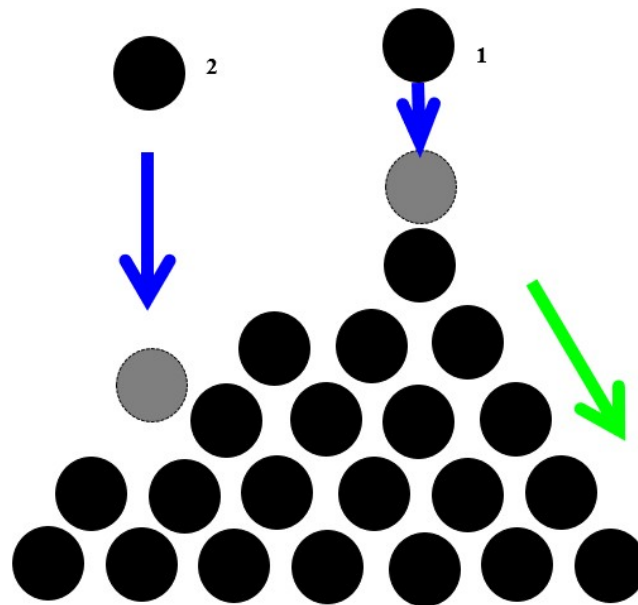


Figure 6.1. The sand-pile conceptual model of SOC. The pile tends to have slope angle defined by the friction between grains. Adding one new grain to the pile may have no effect (grain is at rest) or it may cause an avalanche. The magnitude and frequency of avalanches are inversely related.

The best-studied example of SOC is the “sandpile model,” which represent a conical pile of sand with new grains of sand randomly placed into the pile (**Fig. 6.1**). When the slope exceeds a threshold value (the critical slope angle is related to the coefficient of dry friction between the grains), a grain would move down the slope. Placing a random grain at a particular site may have no effect, or it may trigger an avalanche that will affect many sites at the lattice. Thus, the response

does not depend on the details of the perturbation. It is worth mentioning that the scale of the avalanche is much greater than the scale of the initial perturbation.

There are typical external signs of an SOC system, such as the power-law behavior (the magnitude distribution of the avalanches) and the ‘one-over-frequency’ noise distribution (Bak, 1996). The concept has been applied to such diverse fields as physics, cellular automata theory, biology, economics, sociology, linguistics and others.

It was proposed that SOC plays a role in the formation of brain neural network (*Kozma et al., 2005*). The neural connectivity is sparse at the embryonic stage. After the birth, the connectivity increases and ultimately reaches a certain critical level, at which the neural activity becomes self-sustaining. The brain tissue as a collective system is at the edge of criticality. The combination of structural properties and dynamical factors, like noise level and input gain, the system may transit between subcritical, critical, and supercritical regimes. This mechanism is illustrated in **Fig. 6.2**. The network evolves toward regions of criticality or edge-of-criticality. Once critical regions are established, the connectivity structure remains essentially unchanged. However, by adjusting the noise and/or gain levels, the system can be steered towards or away from critical regions.

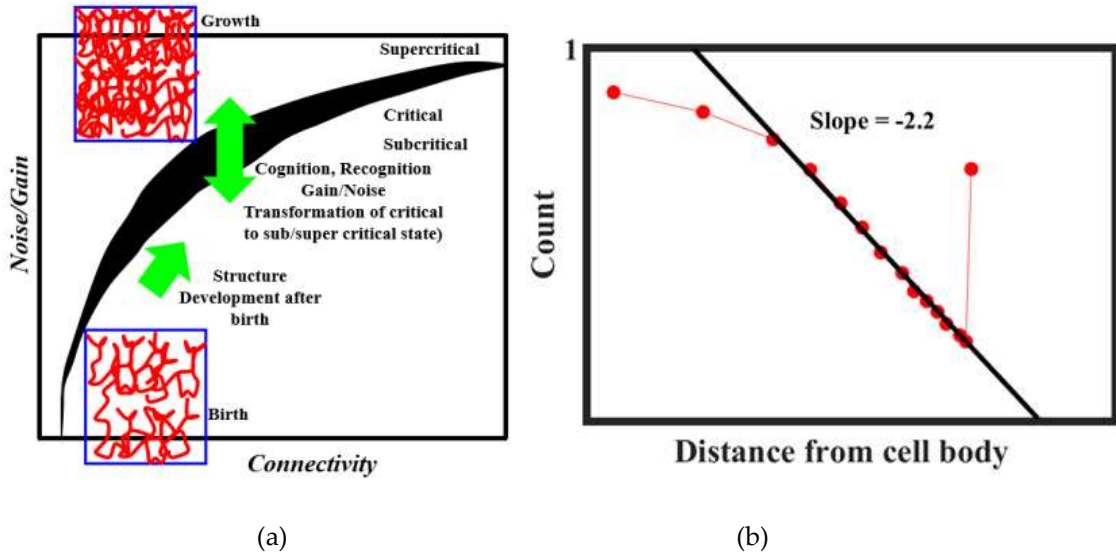


Figure 6.2. Hypotheses of brain network formation by SOC (Kozma et al., 2005). (a) The neocortex network evolves after the birth toward regions of criticality. Once the critical regions (black) are established, the connectivity structure remains essentially unchanged, but it can adjust close to critical regions. (b) Schematic (log-log scale) showing distribution of pyramidal axon tree size. The power law is a typical SOC footprint.

Another important concept, which is related to SOC, is the percolation. Typically, during percolation a certain controlled parameter is slowly changed, for example, nodes are removed from a network or conducting sites are added (Fig. 6.3a), or shear force is increased in a system with friction. When a critical value of the controlled parameter is achieved, the avalanche can be triggered and a corresponding output parameter, such as the correlation length, may reach the infinity (Fig. 6.3b). The correlation length can characterize, for example, the average size of black or white islands on a field of the opposite color, when random pixels are added (Fig. 6.3c). At the critical point, the configuration is fractal (an infinite set of white islands on the black background forming larger black islands on the white background, and so on).

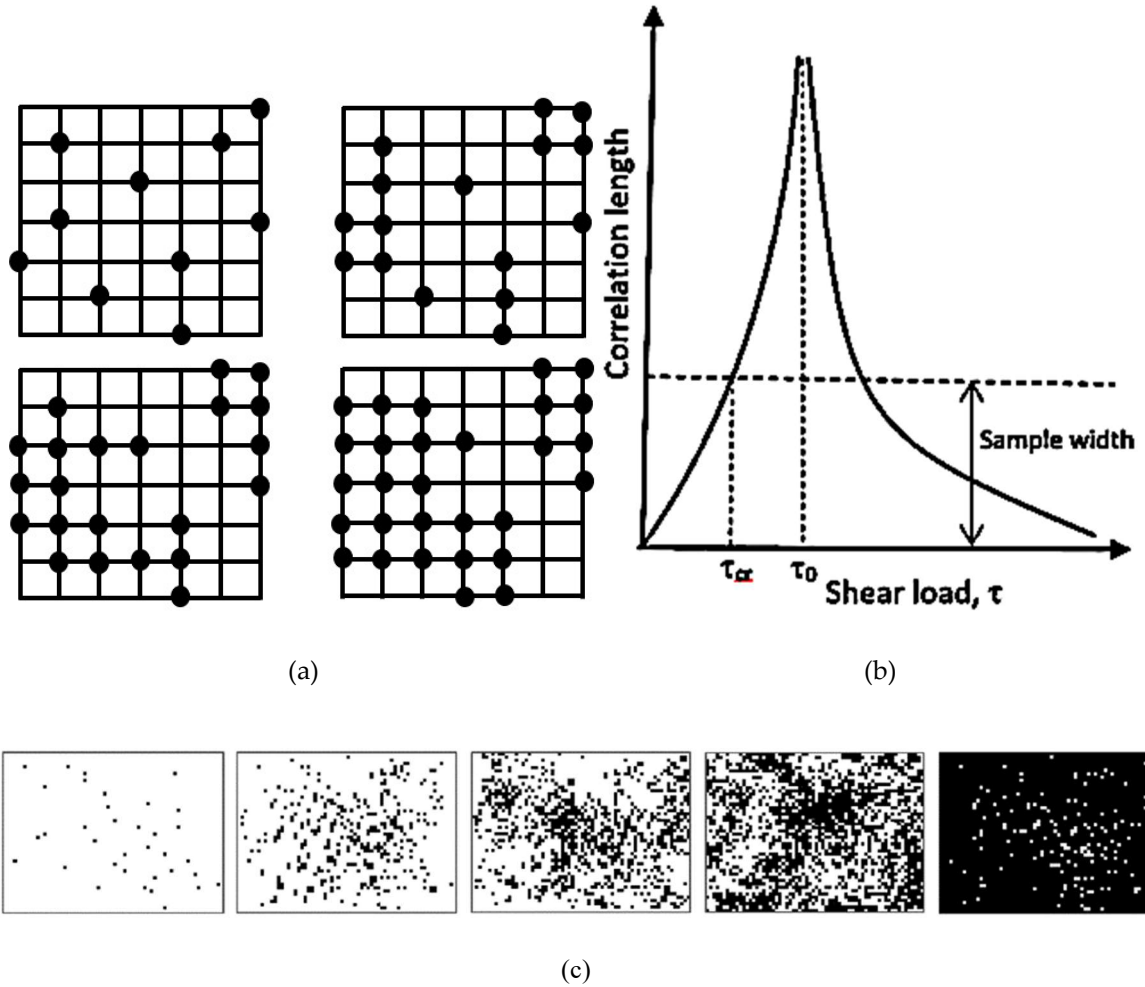


Figure 6.3. Percolation. (a) A 2D torus model with a two active neighbors local update rule showing first four iteration steps at the eighth step all sites become active (*Bollobas, 2001*). (b) A typical dependency of the correlation length on the shear load for an avalanche. At the critical value of the load, τ_0 , the correlation length approaches the infinity. (c) With increasing normal load, the size of slip zone spots (black) increases. A transition to the global sliding is expected when the correlation length approaches the infinity.

Avalanches a common characteristic of brain signals, along with the so-called bursting (*Izhikevich, 2006; Beggs, 2007*). Neural avalanches show characteristics typical for SOC, such as

power-law or one-over-frequency distributions (**Fig. 4.6a**). It is believed that whether the avalanche occurs depends on the branching regime during the neuron connection (**Fig. 4.6b**).

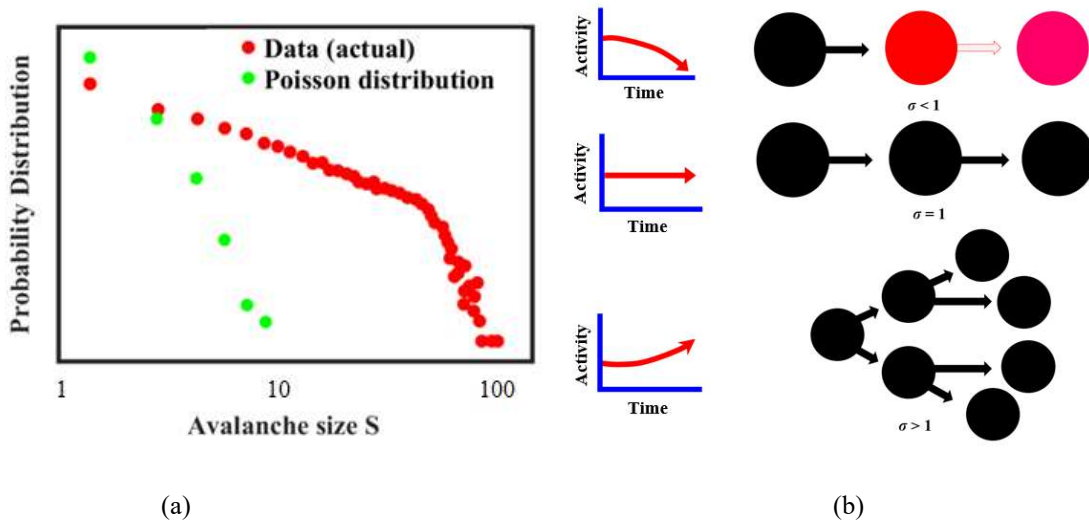


Figure 4.6. (a) Avalanche size (log-log scale) distributions in brain shows a power-law dependency (b)The activity may decrease, stay at the same level, or grow with time depending on the branching regime (*Beggs, 2007*).

6.2. Percolation in multiphase system

The question of to what extent the brain wiring is coded in the DNA remains controversial. The human brain cortex contains at least 10^{10} neurons linked by more than 10^{14} synaptic connections, while the number of base-pairs in a human genome is only 0.3×10^{10} . It is therefore impossible that the information about all synaptic connections is contained in the DNA. Currently, two concepts, namely, the *Protomap* hypothesis and the *Radial Unit* hypothesis, which complement each other, are employed to explain the formation of the neo-cortex. Both hypotheses were suggested by *Pasko Rakic (1995)*.

The *Protomap* is a term for the original molecular “map” of the mammalian cerebral cortex with its functional areas during early embryonic development when neural stem cells are still the dominant cell type. The Protomap is patterned by a system of signaling centers in the embryo, which provide information to the cells about their position and development. This process referred to as the “cortical patterning.” Mature functional areas of the cortex, such as the visual, somatosensory, and motor areas are developed through this process.

During the mammalian evolution, the area of the cortical surface has increased by more than 10^3 times, while its thickness did not change significantly. This is explained by the *Radial Unit Hypothesis* of cerebral cortex development, first described by *Pasko Rakic (1995)*. According to this hypothesis, the cortical expansion is the result of the increasing number of radial columnar units. The increase occurs without a significant change in the number of neurons within each column. The cortex develops as an array of interacting cortical columns or the radial units during embryogenesis. Each unit originates from a transient stem cell layer. The regulatory genes control the timing and ratio of cell divisions. As a result, an expanded cortical plate is created with the enhanced capacity for establishing new patterns of connectivity that are validated through natural selection (*Mountcastle 1997*).

An interesting observation about the human connectome was made by *Kerepesi et al. (2016)*. By analyzing the computer data of the “Budapest Reference Connectome,” which contains macroscale connectome data for 418 individuals, they identified common parts of the connectome graphs between different individuals. It was observed that by decreasing the number of individuals possessing the common feature from 418 down to 1, more graph edges appeared. However, these new appearing edges were not random, but rather similar to a growing “shrub.” The authors called the effect the Consensus Connectome Dynamics and hypothesized that this graph growth may

copy the temporal development of the connections in the human brain, so that the older connections are present in a greater number of subjects.

An important model was suggested recently by *Barabási and Barabási (2020)* who attempted to explain the neuronal connectivity diagram of the *C. elegans* nematode worm by considering neuron pairs that are known to be connected by chemical or electrical synapses. Since synaptic wiring in the *C. elegans* is mostly invariant between individual organisms, it is believed that this wiring is genetically encoded. However, identifying the genes that determine the synaptic connections is a major challenge. *Barabási and Barabási (2020)* identified a small set of transcription factors responsible for synapses formation of specific types of neurons by studying bicliques in *C. elegans*' connectome. According to their model, a set of $\log_2(N)$ transcription factors is sufficient to encode the connection, if transcription factors are combined with what they called the biological operators.

6.3. Percolation and information processing

While identifying parts of the brain responsible for higher order brain activity, such as cognition or speech, and understanding their mechanisms remains a remote (if at all solvable) task, a number of significant observations has been made in the past 20 years. Thus, in the 1990s, B. Biswal, a graduate student at the Medical College of Wisconsin (MCW), discovered that the human brain displays so-called resting state connectivity, observable in the fMRI scans. The phenomenon was later dubbed the Default Mode Network (DMN) and it describes brain functions of a resting state. The DMN is most commonly active when a person is not focused on the outside world and the brain is at wakeful rest, such as during daydreaming and mind-wandering. It is also active when individuals are thinking about others, thinking about themselves, remembering the past, and planning for the future. The DMN has been shown to be negatively correlated with other

networks in the brain such as attention networks, although the former can be active in certain goal-oriented tasks such as social working memory or autobiographical tasks.

Several recent studies have concentrated upon such intriguing features of the DMN as its relationship to the perception of events as a temporal sequence as well as to its role in speech and language-related cognition. These features are of particular interest to the philosophy of mind because language, the ability to plan activities, introspection, and understanding the perspective of another person are often described as distinct characteristic features of humans, which separate them from other mammals.

Konishi et al (2015) investigated the hypothesis that the DMN allows cognition to be shaped by memory-stored information rather than by information in the immediate environment, or, in other words, by “past” rather than by “now”. Using the fMRI technique, they investigated the role of the DMN when people made decisions about where a shape was, rather than where it is now. The study showed that DMN hubs are responsible for the cognition guided by information belonging to the past or to the future, instead of by immediate perceptual input. On the basis of these observations, *Konishi et al. (2015)* suggested that the DMN is employed for higher order mental activities such as imagining the past or future and considering the perspective of another person. These complex introspective activities depend on the capacity for cognition to be shaped by representations that are not present in the current external environment.

In a different study, *Lerner et al. (2011)* investigated how human activities involving integration of information on various time-scales are related to the DMN activation. During real-time lasting activities, such as watching a movie or engaging in conversation, the brain integrates information over multiple time scales. The temporal receptive window (the length of time before a response during which sensory information may affect that response) becomes larger when

moving from low-level sensory to high-level perceptual and cognitive areas. *Lerner et al. (2011)* showed that the temporal receptive window has a hierarchical organization with levels of response to the momentary input, to the information at the sentence time scale, and to the intact paragraphs were heard in a meaningful sequence. The researchers further hypothesized that the processing time scale is a functional property that may provide a general organizing principle for the human cerebral cortex.

In a neurolinguistics study, *Honey et al. (2012)* performed a fMRI research to figure out whether different languages affect different patterns in neural response. They made bilingual listeners to hear the same story in two different languages (English and Russian). The story evoked similar brain responses, which were invariant to the structural changes across languages. This demonstrated that the human brain processes real-life information in a manner that is largely insensitive to the language in which that information is conveyed. *Simony et al. (2015)* further investigated how the DMN reconfigure to encode information about the changing environment by conducting fMRI while making subjects listen to a real-life auditory narrative and to its temporally scrambled versions. The momentary configurations of DMN predicted memory of narrative segments. These are interesting studies which may provide insights into such questions as how the natural language is related to the hypothetical language of thought, which has been postulated by some cognitive scientists and philosophers of language.

7. Scaling in brain networks

In this section we will review current experimental data about scaling properties of cortical networks related to their spatial and temporal organization and their informational content from

the entropic viewpoint. There are several approaches to what constitutes a “time constant” for the brain and how this time constant (i.e., the rate of neural processes) scales with the size of an animal.

7.1. Some experimental observations on scaling in brain networks

Brain networks show a number of remarkable properties. One important experimental observation is that despite the difference in their size by 10^4 times from mouse to whale, mammalian brains tend to operate at almost the same time scales. This can be called the law of conservation of the characteristic time scale. There are two approaches to the characterization of the time scale of brain activity of different creatures: studying brain waves (rhythms of oscillation) and investigations of the critical flicker fusion (CFF) thresholds. The CFF is defined as the frequency of an intermittent light, at which the light appears steady to a human or animal observer (similar to frames in the cinema). It has been hypothesized that the ability of an animal to change body position or orientation (manoeuvrability) is related to the ability to resolve temporal features of the environment and eventually to the CFF (*Healy et al., 2013*). Manoeuvrability usually decreases with increasing body mass.

Buzsáki et al. (2013) reviewed temporal scaling properties of cortical networks by studying hierarchical organization of brain rhythms in mammals. Brain is known to generate electromagnetic oscillations of different frequencies, which can be observed with the EEG. While the exact nature and function of these oscillations remains debatable, they are highly reproducible and classified by their frequencies: alpha-waves (7 – 15 Hz), beta-waves (15 – 30 Hz), gamma-waves (>30 Hz), and others. The frequency of brain oscillations covers almost five orders of magnitude, from <0.01 Hz to hundreds of Hz. The power distribution of brain oscillations tends to show the $1/f^n$ noise spectrum when measured at long scale ranges (*Nunez, 1981*). As we have discussed in the preceding sections, such distribution spectrum is a signature of SOC. However, when specific brain activities are considered, such as concentrating on particular features, moving

or orienting in space or various cognitive functions, particular oscillation frequencies become dominant and the spectrum deviates from the $1/f$ statistics, showing peaks at some characteristic frequencies. These frequencies of various rhythm classes do not vary significantly with the size of the brain (*Buzsáki et al., 2013*).

As far as modeling the origin of oscillations, several dynamic models have been employed to study brain rhythms at various scales and, in particular, at the mesoscale. Thus, the so-called Freeman's K -sets model follows the Katzir-Katchalsky suggested treatment of cell assemblies using network thermodynamics. Hierarchical models of several layers of these sets, from K -I to K -V, provide a modeling tool to conduct analyses of the unifying actions of neocortex related to intentional and cognitive behaviors (*Freeman, 2007*).

The correlation of spatial and temporal brain activity organization was studied by *Honey et al. (2007)*. They related the spontaneous cortical dynamics to the underlying anatomical connectivity at multiple temporal scales. Structural (spatial) hubs corresponded to the hubs of the long-run (minutes) neural activity. For the activities with shorter characteristic time (seconds) significant deviations from special hubs were observed. At the shorter time scale (fraction of a seconds), individual episodes of interregional phase-locking were detected.

The critical flicker fusion threshold is viewed by many researchers as the timescale (or frequency) at which the brain operates. Higher frequency of the CFF threshold implies brain's ability to discern signals and react faster. *Healy et al. (2013)* studied the effect of body mass and metabolic rates of various species on their CFF threshold (**Fig. 7.1**). The comparative metabolic rates are determined separately by measuring oxygen consumption through ventilation (*Makarieva et al. 2008*). It is expected that smaller animals have higher temporal resolution. Larger animals respond to a stimulus slower than the small animals. Therefore, high temporal resolution in large animals

is unnecessary. On the other hand, faster and more manoeuvrable fly species have higher temporal resolutions (Healy *et al.*, 2013), which makes it, for example, so difficult for a human to catch a fly. Note that the mass-specific metabolic rates are almost constant (or, more accurate to say, lie within a certain relatively narrow range) for different life forms with 20 orders of magnitude difference in the body mass (Makarieva *et al.*, 2008). Furthermore, the accuracy of the 3/4-power allometric scaling *Kleiber law* for metabolic rate is not considered universal by some scholars (Glazier, 2005).

We conclude that characteristic frequencies of brain activity are either almost constant or slightly decrease with increasing body and brain size.

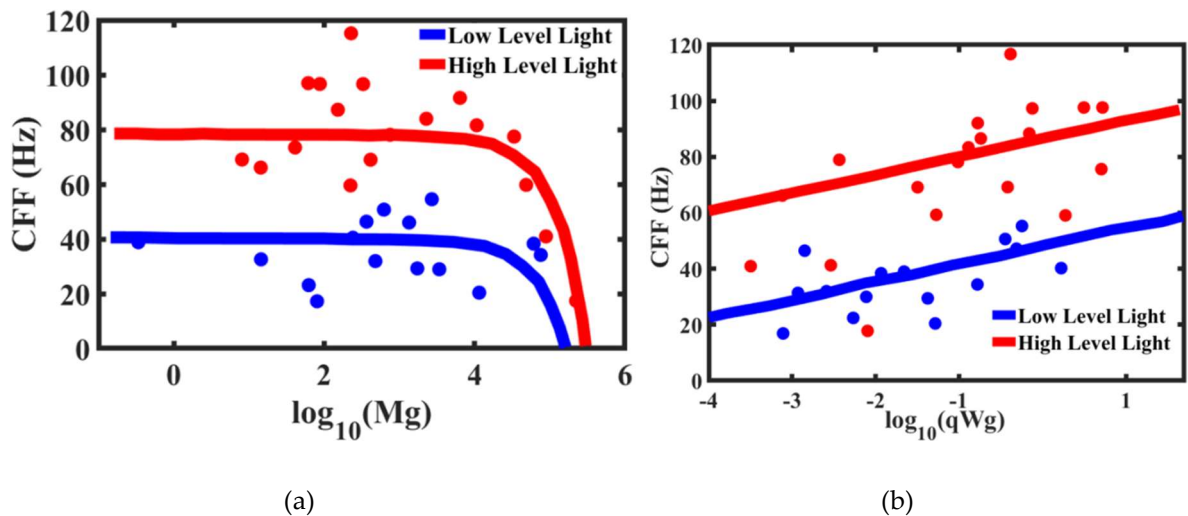


Figure 7.1. The effect of (a) body mass (gram) and (b) temperature-corrected mass-specific resting metabolic rate (qWg) on the CFF shows that the CFF increases with the metabolic rate but decreases with body mass (based on Healy *et al.*, 2013).

7.2. Brain rhythms and scaling

The allometric approach can be applied to the inter-species analysis of brain activity frequencies and time scales in both humans and various species. The observation that typical frequencies of brain activities are often independent of the brain size requires an explanation.

When brains of various species are compared, the distance between homologous regions of brain increases with growing size of the brain. Moreover, the number and length of axons increase even more rapidly than the number of neurons with the growing brain size. Consequently, the average number of synaptic connections in the shortest path between two neurons (the “synaptic path length”) also grows in a very fast manner. Assuming that the cortical network is a scale free and/or a small world network would decrease the path length; however, it does not eliminate completely the scale dependency. The mechanisms which facilitate the increase of signal speed in larger species should be investigated.

Such an investigation was suggested by *Buzsáki et al. (2013)*. The used experimental data about scaling of the brain, in particular, those presented by *Wang et al. (2008)* on the size of axons and the amount of white matter in brain. These are parameters that affect the signal speed. The experimental observations indicate that the increase in axon caliber (size) and their insulation (myelination) compensates for the increased time of signal transfer. The volume of the myelin or white matter in relation to the gray matter (neurons) in the brain scales as power $4/3$ with the size. For instance, while the white matter constitutes 6% of the neocortical volume in hedgehogs, in humans it exceeds 40% of brain volume. This is because a larger brain requires faster signal propagation, and the degree of myelination in larger brains increases.

The velocity of propagation of the neural signal is another significant parameter. *Buzsáki et al. (2013)* noted that for the phase synchronization of gamma-waves in mouse (brain size ~5–10 mm), the speed of conduction of 5 m/s is sufficient, while for humans (70–140 mm) much larger conduction speeds are needed (*Varela et al., 2001*). While increase in conduction velocity can be achieved by both the increase of the volume fraction white matter and axon size, there are several problems associated with this approach.

An increase of axon diameter proportional to the size of the brain would enormously increase brain volume. Experimental observation suggests that, apparently, only a small fraction of all axons have large diameters. Particularly, the largest axons scale linearly with the brain size (**Fig. 7.2**) and they result in an increase of the connection speed. At the same time the required increase of the white matter volume in larger brains does not lead to an unreasonable growth of the volume, because only a small fraction of all axons is large. Consequently, despite a 17,000-fold difference in mammalian brain volumes, the oscillation rhythms with their typical time-scales independent of the brain size are supported by the same mechanisms and they still have the same typical frequencies.

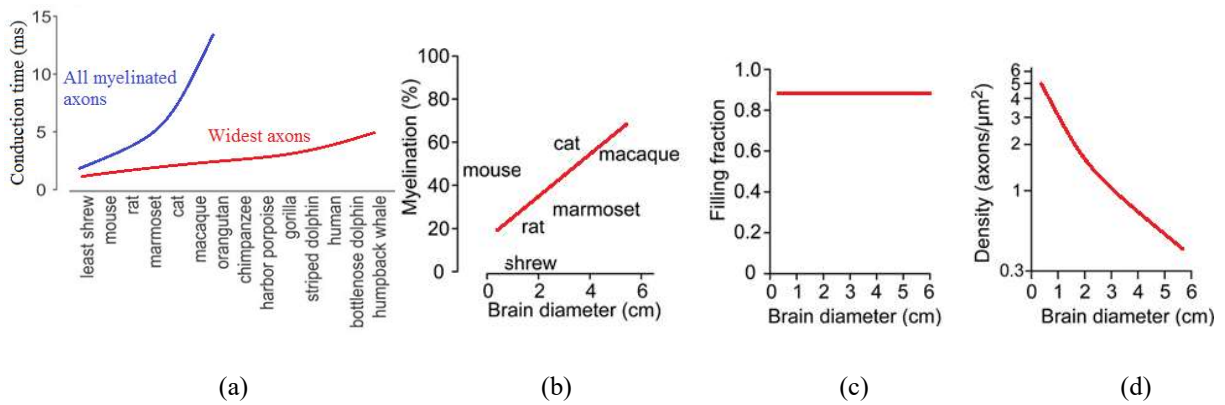


Figure 7.2. Interspecies scaling relations in brain (based on *Wang et al., 2008*). (a) Cross-brain conduction times for myelinated axons; (b) the fraction of myelinated axons; (c) the fraction of volume filled by axons; (d) distribution of axon densities.

The number of nodes, N , scales proportionally to the power D of the characteristic length size of the brain, l , as

$$N \sim l^D \tag{7.1}$$

where D is the fractal dimension of the network. velocity of neural signal propagation is dependent on the ratio $w=W/G$ of the volume fractions of the white matter, W , to the grey matter, G , as a power-function,

$$V \sim w^d \sim \left(\frac{W}{G}\right)^d \quad (7.2)$$

As we have discussed in the preceding sections, in small world networks, the distance between two random nodes is proportional to the logarithm of the total number of nodes,

$$L \sim \ln(N) \sim D * \ln(l) \quad (7.3)$$

The rate of neural processes, i.e., time scale of the brain activity is related to the size of an animal. However, given the experimental observation that the rate is almost a constant independent of the size of the brain, one can assume that the volume fraction of white-to-grey matter affects the velocity of the signal

$$\tau \sim \frac{L}{V} \sim \frac{D * \ln(l)}{\left(\frac{W}{G}\right)^d} = \text{constant} \quad (7.4)$$

From **Eq. 7.4**, it follows immediately that

$$\frac{D * \ln(l)}{\left(\frac{W}{G}\right)^d} = \text{const} \quad (7.5)$$

which can be presented as

$$w = \frac{W}{G} = D^{\frac{1}{d}} * (\ln(l))^{\frac{1}{d}} \quad (7.6)$$

The **Eq. 7.6** relates the ratio of white-to- grey to the characteristic size of the brain. The relationship is plotted in **Fig. 7.3** for the value of $D = 3.2$, for several values of the exponent d . The experimental data, based on *Wang et al., 2008*, for several animals are also presented. It is seen that the best agreement with Eq. 10 is for $2 < d < 3$, which is consistent with the concept that the growth of the white matter content compensates for the increasing linear size of the brain.

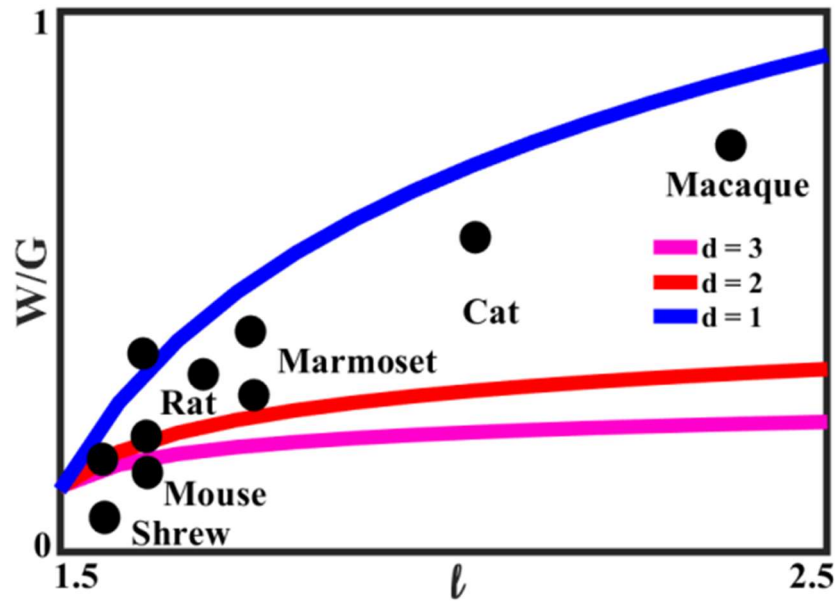


Figure 7.3. Scaling relationship between interspecies brain diameter (cm) and ratio of white & grey matter.

7.3. Information content of the network

The suggestion that brain's connectome as a network possesses topological properties of fractal, scale free, or small-world networks brings a number of interesting questions. The hierarchically organized network with the fractal dimension of d (some estimates state the value of the fractal dimension $d=3.7\pm 0.1$, Klimm et al., 2014) is packed into the 3D cortex, with account of the law of conservation of the characteristic time.

Barabási and Barabási (2020) noted that in order to store the information about the exact structure of the connectome of N neurons, a neuron with k links would need $k \cdot \log_2(N)$ bits of information, with the total information in all neurons $kN \cdot \log_2(N)$. For large organisms this would significantly exceed the information contained in the DNA (**Table 7.1**). Thus, $3.1 \cdot 10^{21}$ bits of information

would be required to characterize the human brain; for comparison, some estimates indicate that human brain memory capacity is 10^{15} - 10^{16} bit, while human genome has about 10^{11} pairs of nucleotides.

To overcome this difficulty, *Barabási and Barabási (2020)* suggested a selective coding model. According to their model, brain cannot encode each link at the genetic level. Instead selective operators are employed, which inspect transcription factor signatures of two neurons (somewhat close in space) and facilitate or to block the formation of a directed link between them. This can be achieved by external agents, like glia cells, which select specific neurons and facilitate synapse formation between them or detect the combinatorial expression of surface proteins, whose protein-protein interactions catalyze synapse formation. The action of such selective operators is evidenced by the emergence of detectable network motifs in the connectome, namely, bicliques.

The model by *Barabási and Barabási (2020)* could provide an insight into the question how much of the information in the structure of the brain is contained in the DNA, and how much is generated during the embryonal and post-embryonal development by self-organizing processes such as SOC. The lower boundary of genetic information can be estimated by the number of transcription factors, T , which encode the identity of a neuron times the total number of neurons.

Table 7.1. Number of neurons, synapses, and corresponding information content of some organisms (based on *Barabási and Barabási, 2020*).

Organism	Neurons, N	Synapses, k	Bits per neuron, $k \cdot \log_2(N)$	Bits per connectome, $kN \cdot \log_2(N)$	Transcription factors, T	Transcription factors information, $N \cdot T$
<i>C. elegans</i>	302	6398	3818	$1.3 \cdot 10^6$	934	$2.8 \cdot 10^5$
<i>Drosophila</i> fruit fly	10^5	10^7	$2.3 \cdot 10^6$	$2.3 \cdot 10^{11}$	627	$6.3 \cdot 10^7$
Mouse	$7.1 \cdot 10^6$	$1.3 \cdot 10^{11}$	$2.6 \cdot 10^8$	$1.9 \cdot 10^{15}$	1457	$1.0 \cdot 10^{10}$
Cat	$7.6 \cdot 10^8$	$6.1 \cdot 10^{12}$	$3.2 \cdot 10^{10}$	$2.5 \cdot 10^{19}$	887	$6.7 \cdot 10^{11}$
Human	$8.1 \cdot 10^9$	$1.6 \cdot 10^{14}$	$3.8 \cdot 10^{11}$	$3.1 \cdot 10^{21}$	1391	$1.1 \cdot 10^{13}$

8. Conclusions

In cardiovascular networks, model of fractal branching relates the ability of such networks to serve homogeneously a 3D volume to the flow through the 2D cross-sections. The West-Brown-Enquist (WBE) model of fractal branching in vascular network explains the empirical allometric law. Despite their wide use, the allometric models raise new concerns, such as the need more accurate accountability for capillary phenomena and more realistic dependencies for the blood flow velocity with decreasing size of vessels. A generalized formulation of the branching model has been suggested in this thesis and the ergodicity of the fluid flow in a vascular network described by such a model was investigated. Generally, the fractal structure of such models makes them non-ergodic, because a particle of the fluid spends more time in small 3D regions comparing with the volumetric fraction of these regions. The time fraction corresponds to the temporal average, while the volumetric fraction corresponds to the spatial average. This mechanism can contribute to the ergodicity breaking in biophysical systems, in addition to such mechanisms as the aging and macromolecular crowding. The non-ergodicity is important for a wide range of biomedical applications where long observations of time series are impractical.

Scaling and dimensional analysis can apply to small clusters of colloidal particles and droplets and to biological networks of neurons connected by synapses, where some properties such as fractal, scale-free and small-world are found. The amount of information contained in a network

could be found by calculating its Shannon entropy. We discussed properties of networks arising from small colloidal particles and droplet clusters due to pairwise interaction between the particles. Many networks found in colloidal science possess self-organizing properties. Examples would be force networks in packed granular material or the sand-pile. Self-organizing systems tune themselves into critical states, which have distinct signatures of fractal dimension and power law (often one-over-frequency) spectrum. We discussed much more complex networks of neurons, which are organized in the neocortex in a hierarchical manner, forming micro- and macro-columns. Scaling relationships in these networks suggest that the characteristic time constant is independent of the brain size when interspecies comparison is conducted. This is because increased diameter of the network is compensated by increasing velocity of the signal due to myelination (insulation of neurons by the white matter). The characteristic time constant can be defined in terms of the frequency of different types of brain waves or as the CFF threshold. Again, the brain networks possess many features including avalanches, fractal topography and on-over-frequency activity. It is interesting to investigate the correlation between the spatial distribution and temporal organization of human brain cognitive activities. The information content of the neural networks could be analyzed using the standard characteristics of the information theory such as Shannon entropy.

9. References

- [1] Arnold V.; Avez A. Ergodic Problems of Classical Mechanics. *Benjamin, New York*. **1968**
- [2] Arnold V. Mathematical methods of classical mechanics. Springer, New York. **1978**
- [3] A.A. Fedorets; E. Bormashenko; L.A. Dombrovsky; M. Nosonovsky. Droplet clusters: nature-inspired biological reactors and aerosols. *Philosophical Transactions of the Royal Society A*. **2019**, 377.
- [4] Aldana M.; Larralde H. Phase transitions in scale-free neural networks: Departure from the standard mean-field universality class. *Phys. Rev. E*. **2004**, 70, 066130.

- [5] A.-L. Barabási; R. Albert. Emergence of scaling in random networks. *Science*. **1999**, 286, 509-512.
- [6] Achard A; Salvador R.; Whitcher B.; Suckling J.; Bullmore E. A Resilient, Low-Frequency, Small-World Human Brain Functional Network with Highly Connected Association Cortical Hubs. *J. Neurosci*. **2006**, 26, 63-72.
- [7] A.A. Fedorets; M. Frenkel; E. Bormashenko; M. Nosonovsky. Small levitating ordered droplet clusters: stability, symmetry, and Voronoi entropy. *The journal of physical chemistry letters*. **2017**, 8 (22), 5599-5602.
- [8] A. M. Makarieva; V. G. Gorshkov; B.-L. Li; S. L. Chown; Peter B. R.; Valery M. G. Mean mass-specific metabolic rates are strikingly similar across life's major domains: Evidence for life's metabolic optimum. *PNAS*. **2008**, 105 (44) 16994-16999.
- [9] Biswal B.; Yetkin F. Z.; Haughton V. M.; Hyde J. S. Functional connectivity in the motor cortex of resting human brain using echoplanar MRI. *Magn Reson Med*. **1995**, 34 (4): 537–541.
- [10] Banavar J.R.; Moses M.E.; Brown J.H.; Damuth J.; Rinaldo A.; Sibly R.M.; Maritan A. A general basis for quarter-power scaling in animals. *Proc. Nat. Acad. Sci*. **2010**, 107.
- [11] Bejan A. The constructal law of organization in nature: tree-shaped flows and body size. *J. Experimental Biol*. **2004**, 208:1677-1686.
- [12] Bejan A. Why the bigger live longer and travel farther: animals, vehicles, rivers and the winds. *Sci. Rep*. **2012**, 2:594.
- [13] Birkhoff G. Proof of the ergodic theorem. *Proc. Natl. Acad. Sci*. **1931**, 17:656-660.
- [14] Bormashenko E.; Voronel A. Spatial scales of living cells and their energetic and informational capacity. *Europ. Biophys. J*. **2018**, 47 (5): 515-521.
- [15] Brown J.H.; West G.B.; Enquist B.J. Yes, West, Brown and Enquist's model of allometric scaling is both mathematically correct and biologically relevant. *Functional Ecology*. **2005**, 19 (4): 735–738.
- [16] Breakspear M.; Stam K.J. Dynamics of a neural system with a multiscale architecture. *Phil. Trans. R. Soc. B*. **2005**, 360: 1051-1074.
- [17] Etienne R.S.; Apol M.E.; Olf H.A. Demystifying the West, Brown & Enquist model of the allometry of metabolism. *Functional Ecology*. **2006**, 20 (2): 394–399.
- [18] Barenblatt, G. I. Scaling, self-similarity, and intermediate asymptotics. *New York: Cambridge University Press: New York*, **1996**
- [19] Balázs S.; Bálint V.; Vince G. The Robustness and the Doubly Preferential Attachment Simulation of the Consensus Connectome Dynamics of the Human Brain. *Sci Rep*. **7**.
- [20] Baruch L.; Itzkovitz S.; Golan-Mashiach M.; Shapiro E.; Segal E. Using Expression Profiles of *Caenorhabditis elegans* Neurons to Identify Genes that Mediate Synaptic Connectivity. *PLoS Comput Biol*. **2008**, 4(7): e1000120.
- [21] Braitenberg V.; Schüz A. Cortex: Statistics and Geometry of Neuronal Connectivity. *2nd edition, Berlin: Springer-Verlag*. **1998**.
- [22] Beggs, J. M.; D. Plenz. Neuronal avalanches in neocortical circuits. *J Neurosci*. **2003**, 23(35): 11167-77.
- [23] Buzsáki G.; Logothetis N.; Singer W. Scaling brain size, keeping timing: evolutionary preservation of brain rhythms. *Neuron*. **2013**, 80(3):751–764.
- [24] Biswal B.; Yetkin F. Z.; Haughton V. M.; Hyde, J. S. Functional connectivity in the motor cortex of resting human brain using echoplanar MRI. *Magn Reson Med*. **1995**, 34 (4): 537–541.
- [25] Cook S.J.; Jarrell T.A.; Brittin, C.A. et al. Whole-animal connectomes of both *Caenorhabditis elegans* sexes. *Nature*. **2019**, 571, 63–71.

- [26] Christopher J. H.; Christopher R. T.; Yulia L.; Uri H. Not Lost in Translation: Neural Responses Shared Across Languages. *J. Neurosci.* **2012**, 32(44):15277–15283
- [27] Cook S.J.; Jarrell T.A.; Brittin C.A. et al. Whole-animal connectomes of both *Caenorhabditis elegans* sexes. *Nature.* **2019**, 571, 63–71
- [28] C. Shan X.; Michal J.; Zhiyuan L. A Connectome of the Adult *Drosophila* Central Brain.
- [29] Cook S.J.; Jarrell T.A.; Brittin, C.A. et al. Whole-animal connectomes of both *Caenorhabditis elegans* sexes. *Nature.* **2019**, 571, 63–71.
- [30] D. L. Barabási; A-L Barabási, A Genetic Model of the Connectome 2020, *Neuron* 105, 1–11
- [31] Daniel P. B.; Manuel F. C. The minicolumn hypothesis in neuroscience. *Brain.* **2000**, 125.
- [32] De Lellis C.; Székelyhidi L. On turbulence and geometry: from Nash to Onsager. *Not. Am. Math. Soc.* **2019**, 05:677-685
- [33] Duncan S.; Callaway M. E.; J. Newman; Steven H. Strogatz, and Duncan J. Watts Network Robustness and Fragility: Percolation on Random Graphs *Phys. Rev. Lett.* **2002**, 85, 5468
- [34] E. Bormashenko; M. Frenkel; A Vilks. A.A. Fedorets; N. E. Aktaev; L. A. Dombrovsky; M. Nosonovsky. Characterization of self-assembled 2D patterns with Voronoi Entropy, *Entropy* **2019**
- [35] Erdős, P.; Rényi, A. On Random Graphs. *Publicationes Mathematicae.* **1959**, 6: 290–297.
- [36] E. Simony; Christopher J. H.; Janice C.; Olga L.; Yaara Y.; Ami W.; Uri H. Dynamic reconfiguration of the default mode network during narrative comprehension. *NATURE COMMUNICATIONS.* **2015**, 7:12141.
- [37] E. Bormashenko; A.A. Fedorets; M. Frenkel; L.A. Dombrovsky; M. Nosonovsky. Clustering and self-organization in small-scale natural and artificial systems. *Philosophical Transactions of the Royal Society A.* **2020**, 378, 20190443
- [38] Eugene M. I. Bursting. *Scholarpedia.* **2006**, 1(3):1300.
- [39] Freeman W.J.; Holmes M.D.; West G.A.; Vanhatalo S. Fine spatiotemporal structure of phase in human intracranial EEG. *Clin Neurophysiol.* **2006**, 117, 6, pp 1228-1243
- [40] Glazier D. S. Beyond the “3/4-power law”: Variation in the intra- and interspecific scaling of metabolic rate in animals. *Biol Rev.* **2005**, 80:611– 662.
- [41] Guzman-Sepulveda, J. et al. Real-time intraoperative monitoring of blood coagulability via coherence-gated light scattering. *Nat. Biomed. Eng.* **2017**, 1. doi:10.1038/s41551-017-0028
- [42] Fabry B.; Maksym G.N.; Butler J.P.; Glogauer M.; Navajas D.; Taback N.A.; Millet E.J.; Fredberg J.J. Time scale and other invariants of integrative mechanical behavior in living cells. *Phys Rev E.* **2003**, 68:041914
- [43] Fedorets A.A.; Bormashenko E.; Dombrovsky L.A.; Nosonovsky M. Droplet clusters: nature-inspired biological reactors and aerosols. *Phil. Trans. R. Soc. A.* **2019a**, 377 (2150): 20190121.
- [44] Fedorets A.A.; Aktaev N.E.; Gabyshev D.N.; Bormashenko E.; Dombrovsky L.A.; Nosonovsky M. Oscillatory Motion of a Droplet Cluster. *J. Phys. Chem. C.* **2019b**, 123 (38): 23572-23576.
- [45] Földes-Papp Z.; Baumann G. Fluorescence molecule counting for single-molecule studies in crowded environment of living cells without and with broken ergodicity. *Current pharmaceutical biotechnology.* **2011**, 12(5): 824–833. doi:10.2174/138920111795470949
- [46] Hasan A.; Paul A.; Vrana N.E.; Zhao X.; Memic A.; Hwang Y.S.; Dokmeci M.R.; Khademhosseini A. Microfluidic techniques for development of 3D vascularized tissue. *Biomaterials.* **2014**, 35: 7308–7325
- [47] Hofling F.; Franosch, T. Anomalous transport in the crowded world of biological cells. *Rep. Prog. Phys.* **2013**, 76: 046602 doi:10.1088/0034-4885/76/4/046602
- [48] Hrnčíř E.; Rosina J. Surface tension of blood. *Physiol Res.* **1997**, 46(4):319-321

- [49] J. S. Andrade Jr; H. J. Herrmann; R. F. Andrade; L. R. de Silva; Apollonian networks: simultaneously scale-free, small world, euclidean, space filling, and with matching graphs. *Phys. Rev. Lett.* **2005**, 94, 018702
- [50] Jonathan C. H.; Daniel L. A. The cortical column: a structure without a function. *Phil. Trans. R. Soc. B.* **2005**, 360, 837–862
- [51] John M. Beggs. Neuronal avalanche. *Scholarpedia.* **2007**, 2(1):1344.
- [52] Kadanoff L.P. More is the Same, Phase Transitions and Mean Field Theories. *J Stat Phys.* **2009**, 137: 777–797
- [53] Kleiber M. Body size and metabolism. *Hilgardia.* **1932**, 6 (11): 315–351
- [54] Kleiber M. Body size and metabolic rate. *Physiol. Rev.* **1947**, 27 (4): 511–41
- [55] Kozlowski J.; Konarzewski M. Is West, Brown and Enquist's model of allometric scaling mathematically correct and biologically relevant? *Functional Ecology.* **2004**, 18 (2): 283–9
- [56] Krishnan A.; Wilson A.; Sturgeon J.; Siedleckia C.A.; Vogler E.A. Liquid–vapor interfacial tension of blood plasma, serum and purified protein constituents thereof. *Biomaterials.* **2005**, 26 (17): 3445-3453
- [57] Kulkarni A.M.; Dixit N.M.; Zukoski C.F. Ergodic and non-ergodic phase transitions in globular protein suspensions. *Faraday Discuss.*, **2003**, 123, 37–50
- [58] Kozma R.; Puljic M.; Balister P.; Bollobas B.; Freeman, W. J. Phase transitions in the neuro percolation model of neural populations with mixed local and non-local interactions. *Biological Cybernetics.* **2005**, 92(6), 367-379.
- [59] Kerepesi C.; Szalkai B.; Varga B.; Grolmusz V. How to Direct the Edges of the Connectomes: Dynamics of the Consensus Connectomes and the Development of the Connections in the Human Brain. *PLoS One.* **2016**, 11(6): e0158680.
- [60] K. Healy; L. McNally; G. D. Ruxton; N. Cooper; A. L. Jackson. Metabolic rate and body size are linked with perception of temporal information. *Animal Behavior.* **2013**, 86 (4), 685-696
- [61] Klimm, F.; Bassett, D. S.; Carlson, J. M.; Mucha, P. J. Resolving structural variability in network models and the brain. *PLoS computational biology.* **2014**, 10(3), e1003491.
- [62] Kozma R.; Puljic M.; Balister P.; Bollobas B.; Freeman W. J. Neuro percolation: A random cellular automata approach to spatio-temporal neuro dynamics. *Lecture Notes in Computer Science.* **2004**, 3305, 435-443. <http://repositories.cdlib.org/postprints/1013/>
- [63] Konishi M.; McLaren D.G.; Engen H.; Smallwood J. Shaped by the Past: The Default Mode Network Supports Cognition that Is Independent of Immediate Perceptual Input. *PLoS One.* **2015**,10(6): e0132209.
- [64] Lim M.X.; Souslov A.; Vitelli V.; Jaeger H.M. Cluster formation by acoustic forces and active fluctuations in levitated granular matter. *Nature Phys.* **2019**, 15: 460–464
- [65] Lichtman J. W.; Sanes J.R. Ome sweet ome: what can the genome tell us about the connectome? *Curr Opin Neurobiol.* **2008**, 18(3):346–353.
- [66] Maani N.; Rayz V.L.; Nosonovsky M. Biomimetic approaches for green tribology: from the lotus effect to blood flow control. *Surface Topography: Metrology and Properties.* **2015**, 3: 034001
- [67] Magdziarz M.; Zorawik T. Lamperti transformation - Cure for ergodicity breaking. *Commun Nonlinear Sci Numer Simulat.* **2019**, 71:202–211
- [68] Manzo C.; Torreno-Pina J.A.; Massignan P.; Lapeyre G.J.; Lewenstein M.; Garcia Parajo M.F. Weak Ergodicity Breaking of Receptor Motion in Living Cells Stemming from Random Diffusivity. *Phys. Rev. X.* **2015**, 5: 011021

- [69] M. Nosonovsky and B. Bhushan, “Do Hierarchical Mechanisms of Superhydrophobicity Lead to Self-organized Criticality?” *Scripta Mater.* **2008**, 59.
- [70] Mountcastle V.B. The columnar organization of the neocortex. *Brain.* **1997**, 120: 701–22
- [71] M. Nosonovsky; A.D. Breki. Ternary logic of motion to resolve kinematic frictional paradoxes. *Entropy.* **2019**, 21 (6), 620
- [72] Marieb E.N.; Hoehn K. The Cardiovascular System: Blood Vessels. *In: Human anatomy & physiology (9th ed.) Pearson Education.* **2013**, p. 712
- [73] M. Nosonovsky. Logical and information aspects in surface science: friction, capillarity, and superhydrophobicity. *International Journal of Parallel, Emergent and Distributed Systems.* **2018**, 33, 07-318
- [74] N. Aktaev.; A. Fedorets.; E. Bormashenko.; M. Nosonovsky. Langevin Approach to Modeling of Small Levitating Ordered Droplet Clusters. *The Journal of Physical Chemistry Letters.* **2019**, 9, 3834–3838
- [75] Nosonovsky and Mortazavi. Friction-induced vibrations and self-organization. *CRC Press.* **2014**.
- [76] Nosonovsky M.; Rohatgi P.K. Biomimetics in Materials Science: Self-Healing, Self-Lubricating, and Self-Cleaning Materials. *Springer, New York.* **2012**.
- [77] Nosonovsky, M.; Mortazavi, V. Friction-induced vibrations and self-organization: mechanics and non-equilibrium thermodynamics of sliding contact. *Boca Raton, FL: CRC Press, Taylor & Francis Group.* **2014**
- [78] Nosonovsky M.; Roy P. Allometric scaling law and ergodicity breaking in the vascular system. *Microfluidics and Nanofluidic-Springer.* **2020**
- [79] Nosonovsky M.; Roy P. Scaling and Entropy in colloidal and neural networks. *Entropy-MPDI.* **2020**.
- [80] O. Gendelman; Y. G. Pollack; I. Procaccia; S. Sengupta; J. Zylberg, What Determines the Static Force Chains in Stressed Granular Media? *Phys. Rev. Lett.* 116, 078001
- [81] P. Rakic. A small step for the cell, a giant leap for mankind: a hypothesis of neocortical expansion during evolution. *Trends in Neurosciences.* **1995**, 18 (9): 383–8.
- [82] Rakic P. Evolution of the neocortex: a perspective from developmental biology. *Nat Rev Neurosci.* **2009**, 10(10):724–735.
- [83] Ramachandran R.; Maani N.; Rayz V.L.; Nosonovsky M. Vibrations and spatial patterns in biomimetic surfaces: using the shark-skin effect to control blood clotting. *Phil. Trans. R. Soc. A.* **2016**, 374: 20160133
- [84] Rakic P. Specification of cerebral cortical areas. *Science.* **1988**, 241 (4862): 170–6.
- [84] Rypina I.I.; Scott S.E.; Pratt L.J.; Brown M.G. Investigating the connection between complexity of isolated trajectories and Lagrangian coherent structures. *Nonlin. Processes Geophys.* **2011**, 18: 977–987
- [85] R. Kozma. Neuro percolation, *Scholarpedia*, **2007**, 2(8):1360.
- [86] R. C. Hardie; K. Franze. Photomechanical Responses in Drosophila Photoreceptors. *Science.* **2012**, 338 (6104) 260-263.
- [87] Reuven C.; Keren E.; Daniel ben-A.; Shlomo H. Resilience of the Internet to Random Breakdowns. *Phys. Rev. Lett.* 85, 4626
- [88] R. Albert; A.L. Barabási. Statistical mechanics of complex networks. *Reviews of Modern Physics.* **2002**, 74, 47–97.

- [89] R. W. Perry; M. C. Holmes-Cerfon; M. P. Brenner; V. N. Manoharan. Two-Dimensional Clusters of Colloidal Spheres: Ground States, Excited States, and Structural Rearrangements. *PRL*. **2015**, 114, 228301.
- [90] Savage V.M.; Gillooly J.F.; Woodruff W.H.; West G.B.; Allen A.P., Enquist B.J.; Brown J.H. The predominance of quarter-power scaling in biology. *Functional Ecology*. **2004**, 18 (2): 257–282
- [91] Sporns O.; Zwi J.D. The small world of the cerebral cortex. *Neuro Informatics*. **2004**, 4: 145-162.
- [92] Savage V.M.; Deeds E.J.; Fontana W. Sizing Up Allometric Scaling Theory. *PLoS Comput. Biol.* **2008**, 4(9): e1000171.
- [93] Scott S.E.; Redd T.C.; Kuznetsov L.; Mezić I.; Jones C.K.R.T. Capturing deviation from ergodicity at different scales. *Physica D: Nonlinear Phenomena*. **2009**, 238 (16):1668-1679
- [94] Shnirelman A. Weak Solutions with Decreasing Energy of Incompressible Euler Equations. *Comm Math Phys*. **2000**, 210: 541-6-3
- [100] T. S. Majmudar; R. P. Behringer. Contact force measurements and stress-induced anisotropy in granular materials, *Nature (London)*. **2005**, 435, 1079.
- [101] Thurston G.B. Viscosity and viscoelasticity of blood in small diameter tubes. *Microvascular Research*. **1976**, 11:133-146
- [102] Varela F.; Lachaux J.P.; Rodriguez E.; Martinerie J. The brain-web: phase synchronization and large-scale integration. *Nat Rev Neurosci*. **2001**, 2:229–239
- [103] West G.B.; Brown J.H.; Enquist B.J. A general model for the origin of allometric scaling laws in biology. *Science*. **1997**, 276 (5309): 122–6
- [104] Wang S.S.; Shultz J.R.; Burish M.J.; Harrison K.H.; Hof P.R.; Towns L.C.; Wagers M.W.; Wyatt K.D. Functional trade-offs in white matter axonal scaling. *J Neurosci*. **2008**, 9, 28(15):4047-56.
- [105] Walter J. Freeman. Michael Breakspear. Scale-free neocortical dynamics. *Scholarpedia*. **2007**, 2(2):1357. http://www.scholarpedia.org/article/Scale-free_neocortical_dynamics
- [106] Watts D. J; Strogatz S. H. Collective dynamics of 'small-world' networks. *Nature*. **1998**, 393 (6684): 440–2
- [107] Yulia L.; Christopher J. H.; Lauren J. S.; Uri H. Topographic Mapping of a Hierarchy of Temporal Receptive Windows Using a Narrated Story. *The Journal of Neuroscience*. **2011**, 31(8):2906 –2915
- [108] Yun-Tao Liu; Chang-Lu Tao; Xiaokang Zhang; Lei Qi; Rong Sun; Pak-Ming Lau; Z. Hong Zhou; Guo-Qiang Bi. Mesophasic organization of GABAA receptors in hippocampal inhibitory synapse. **2020**. doi: <https://doi.org/10.1101/2020.01.06.895425>